Subsurface Valleys and Geoarcheology of the Eastern Sahara Revealed by Shuttle Radar

Abstract. *The shuttle imaging radar (SIR-A) carried on the space shuttle Columbia in November 1981 penetrated the extremely dry Selima Sand Sheet, dunes, and drift sand of the eastern Sahara, revealing previously unknown buried valleys, geologic structures, and possible Stone Age occupation sites. Radar responses from bedrock and gravel surfaces beneath windblown sand several centimeters to possibly meters thick delineate sand- and alluvium-filled valleys, some nearly as wide as the Nile Valley and perhaps as old as middle Tertiary. The now-vanished major river systems that carved these large valleys probably accomplished most of the erosional stripping of this extraordinarily flat, hyperarid region. Underfit and incised dry wadis, many superimposed on the large valleys, represent erosion by intermittent running water, probably during Quaternary pluvials. Stone Age artifacts associated with soils in the alluvium suggest that areas near the wadis may have been sites of early human occupation. The presence of old drainage networks beneath the sand sheet provides a geologic explanation for the locations of many playas and present-day oases which have been centers of episodic human habitation. Radar penetration of dry sand and soils varies with the wavelength of the incident signals (24 centimeters for the SIR-A system), incidence angle, and the electrical properties of the materials, which are largely determined by moisture content. The calculated depth of radar penetration of dry sand and granules, based on laboratory measurements of the electrical properties of samples from the Selima Sand Sheet, is at least 5 meters. Recent (September 1982) field studies in Egypt verified SIR-A signal penetration depths of at least 1 meter in the Selima Sand Sheet and in drift sand and 2 or more meters in sand dunes.*

During its second test flight, in November 1981, the space shuttle Columbia carried the shuttle imaging radar (SIR-A) experiment over the core of the largest expanse of hyperarid terrain on the earth and one of the last places to be explored extensively by conventional geologic techniques. Because this region now lacks almost any surficial traces of fluvial processes and is dominated by eolian erosional and depositional activity, it has been given a special name to distinguish it from the rest of the Sahara. Since the beginning of scientific exploration of the general region by Rohlfs (*1*), numerous workers have pointed out its unusual character. Rainfall at any locality occurs at about 30- to 50-year intervals, based on botanical evidence and the state of preservation of recent artifacts such as gasoline cans, food tins, newspapers, cigarette packages, vehicles, and their still clearly preserved tracks, all left from explorations and military activities before and during the early part of World War II (C.V.H., unpublished data).

Haynes (*2*) has proposed the name Darb el Arbain (Forty Days Road) Desert for this inhospitable region, which is now uninhabited except for some of the major oases. The region owes its present hyperaridity to distance from the moist summer winds that move into North Africa from the South Atlantic, and to its position far south of the storm tracks that move across the Mediterranean during winter. The 200-mm precipitation isohyet, which marks the northern edge of the tropical savanna zone in North Africa, lies about 800 km south of the central Arbain region (Fig. 1); that this was not always the case in the past has been shown by numerous paleoclimatic studies (*3, 4*). The Arbain Desert is roughly defined (*2*) as the area south of the Limestone Plateau, west of the Nile Valley, east of the Libya and Chad borders, and north of Wadi Howar in the Sudan. It is named after the ancient but still used camel caravan route (the Darb el Arbain) that traverses the region from El Fasher to the Kharga Depression; presently inhabited oases in the Kharga and Dakhla depressions mark its approximate northern extent (Fig. 1). The SIR-A track enters the Arbain Desert at the Chad-Sudan border, traverses the little-known region north of Merga and south of the Gilf Kebir plateau and Gebel Uweinat, enters Egypt south of Bir Sahara, and exits from the Arbain Desert northeast of Bir Kiseiba.

General description of area. The Arbain Desert is floored mostly by Cretaceous Nubia Formation made up of cross-bedded sandstones and shales whose clastic units are informally known as Nubian sandstones, and by low sporadic outcrops of granite and granitic gneiss of the Precambrian African shield (*5, 6*). Outcrops are typically extensively wind-pitted, grooved, and fluted to the point that they resemble the rocks seen by the Viking Landers on Mars (Fig. 2a) (*7, 8*). Surface evidence for the former presence of major integrated drainage systems is virtually absent. Vegetation is also almost entirely absent except at the minor oases or wells known as "birs" (Fig. 1 and Fig. 2c). The desert floor is mostly covered by yellowish to slightly reddish windblown sand in extensive, thin, flat to undulating sheet deposits with occasional giant trains, many tens of kilometers long, of simple and compound barchanoid dunes (Fig. 2d). Inselbergs without pediments (conical hills, Fig. 2e), low outcrops, occasional lake bed deposits, and patches of gravel ventifacts punctuate the otherwise monotonous and barren landscape (Fig. 2, f to h).

The area is classic for the clarity of its Quaternary climatic cycles. General aridity set in during the beginning of the Pleistocene, but abundant evidence of episodic human occupation is present in the form of widely distributed Acheulean implements (200,000 ± 100,000 years old), several periods of Mousterian and Aterian occupation (100,000 to 40,000 years ago), and reoccupation by Late Paleolithic and Neolithic people (about 10,000 years ago). These Quaternary episodes of human occupation coincide with the so-called pluvial conditions that produced at best a savanna-like environment, but which allowed many small playas and intermittent streams to exist; it is around such water sources that many habitation sites have been found. Domesticated animals appeared (Fig. 3a) and agriculture was practiced locally (*9*). By about 5000 years ago hyperaridity set in again and the Arbain Desert was essentially abandoned.

Since the late 19th century, the Arbain Desert has been the object of many expeditions and much geological and archeological work. Most of us had the opportunity to work in the Arbain Desert with numerous colleagues during expeditions in 1978, 1980, and 1982, while studying possible analogs of Martian landforms (*10, 11*). Serendipitously, the paths of our expeditions passed many times under the eventual track of the SIR-A experiment (Fig. 1). A somewhat tentative picture of the previous role of fluvial activity in shaping this now predominantly eolian landscape emerged from the results of our earlier work, and this picture has been strengthened by the radar images.

Of particular importance in the part of the SIR-A track that we have examined—parts of the area from northwest Sudan to the edge of the Limestone Plateau northeast of Bir Kiseiba—is the Selima Sand Sheet (Fig. 2d and Fig. 3, b and c). This is one of the most barren, featureless expanses of terrain on the earth (12). Its windblown surface consists of sand and fine granules, with local patches of what appear to be wind-truncated granule ripples and gravel ventifacts. For hundreds of kilometers it is almost completely flat; in places it is gently rolling, but relief is hardly more than about 10 m. Numerous test pits dug by Haynes and others during several expeditions across the Arbain Desert (Fig. 3, b and c) reveal that the Sand Sheet consists of unweathered, finely laminated eolian sand that is commonly less than 10 cm and generally no more than a few meters thick. In many localities the sand overlies yellowish-red to markedly reddened, pebbly alluvium (11). Some of the soils in the alluvium

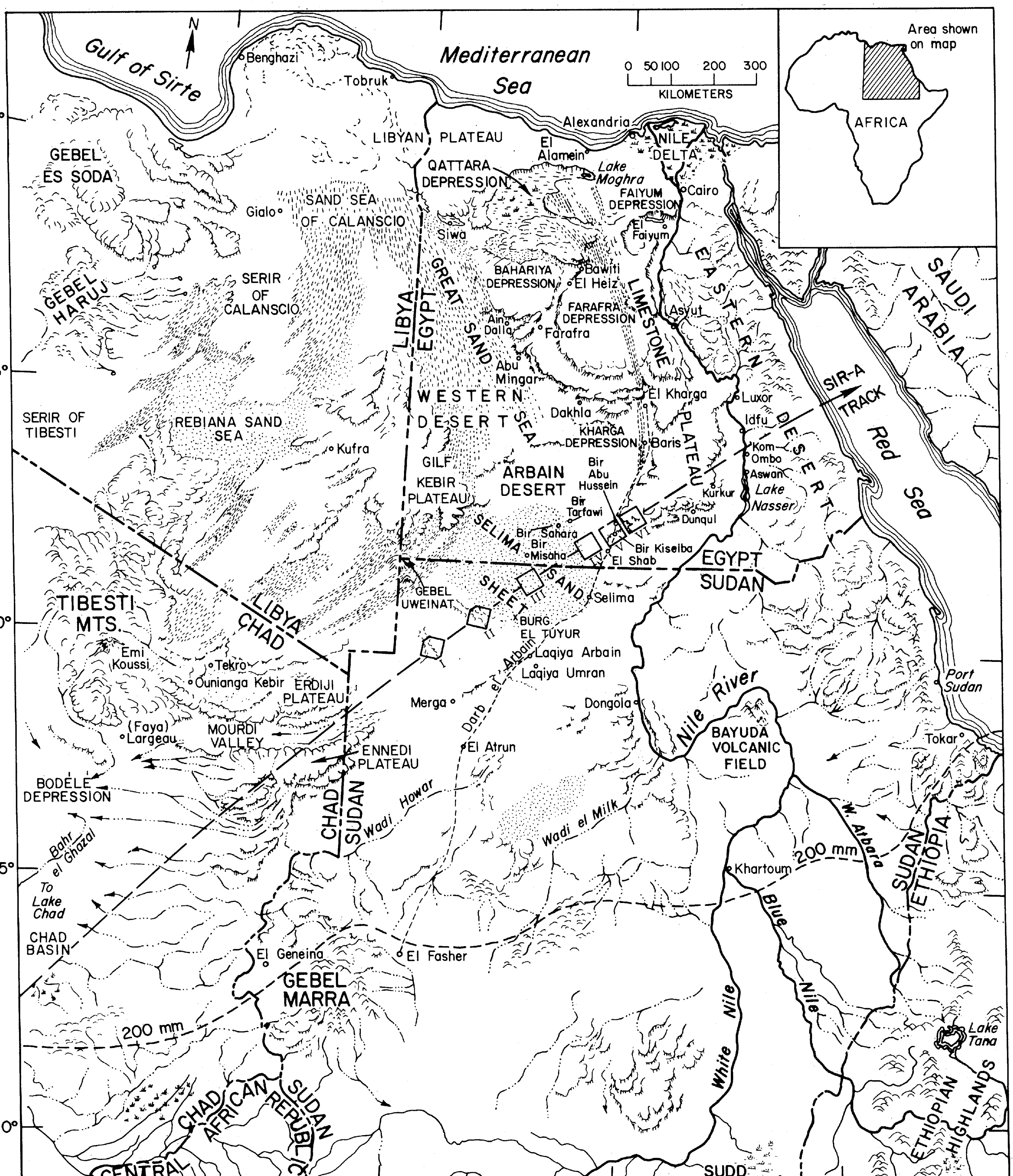

Fig. 1. Index and generalized topographic map of the eastern Sahara, showing location of the SIR-A track and areas I to VI along this swath, which were mapped and analyzed in detail (Figs. 4 to 9). Areas to the north of the precipitation isohyet (76) receive less than 200 mm annual rainfall. [Redrawn by R. Sabala, in part after Raisz (35)]

have been dated (from artifacts and ostrich egg shells) at about 8500 years before present (*12*). The Selima Sand Sheet, many of the smaller dunes migrating across it, and varying thicknesses of drift sand in the Arbain Desert were penetrated by SIR-A, revealing a dramatically different and predominantly fluvial subsurface terrain known previously only to the Stone Age peoples and possibly earlier hominids of the region.

Paleodrainage based on previous work. Recent studies in southwest Egypt have shown that major integrated stream systems once debouched from the now nearly defunct wadis of the 1200 km^2, 300-m-high Gilf Kebir plateau (Fig. 1) onto the essentially flat plain that floors the Arbain Desert. Several of these now defunct stream systems were reconstructed by tracing their apparent courses between remnant interfluves recognized on Landsat images (*13, 14*) processed by methods summarized by Chavez *et al.* (*16*). One of these stream networks, informally named Wadi Eight Bells (*16*), drained an area of at least 3400 km^2 on the pediplane south of the Gilf Kebir plateau. The former course of this master stream was traced southward on Landsat images to about 200 km beyond the presently retreating scarp of the plateau and to within 200 km of the SIR-A track in the northwest Sudan. This work led to the suggestion that the Gilf Kebir is a relict drainage divide that dates from the beginning of the erosional stripping of Tertiary, Mesozoic, and Paleozoic strata from south-central Egypt which followed the retreat of late Eocene seas from the eastern Sahara (*13–15, 17*).

Courses of now defunct streams that flowed north from the Gilf, and probably carried some of the sand now migrating southward in the Great Sand Sea, have been recognized from ground and Landsat observations by Haynes (*12*) and Issawi (*18*); this further strengthens the concept of the Gilf Kebir as a major drainage divide in the Arbain Desert and indeed in the entire eastern Sahara of western Egypt, eastern Libya, and northwest Sudan. Farther west, Pachur (*19*) has discovered a similarly large, integrated "fossil" drainage system, probably of late Quaternary age, that formerly emanated from the north flanks of the Tibesti Mountains (Fig. 1) and can be traced northward for more than 1000 km, toward the Gulf of Sirte.

Before discussing the SIR-A results related to the paleodrainage in the eastern Sahara, we must briefly mention the current state of knowledge about the evolution of the Nile River east and south of the Arbain Desert (Fig. 1). This work has been summarized by Said (*20*); it was built on the efforts of hundreds of workers dating back to the cartographers and engineers of the French expedition to Egypt in 1778 to 1799, and was earlier synthesized by Butzer and Hansen (*21*). The physical history of the Nile in the Sudan has been reviewed by Berry and Whiteman (*22*). The following account is based mainly on Said's (*20*) conclusions [geologic ages given in parentheses are from Van Eysinga (*23*)].

After the retreat of the sea from northeast Africa at the end of the Eocene epoch (about 40 million years ago), rivers of Oligocene age contributed to widespread denudation of the region; deposits of fluvial sands, flint cobbles, and petrified wood are identified from this long, humid episode. Both Oligocene and Miocene time (about 38 million to 5 million years ago) were marked by extensive volcanism and tectonic disturbances; little is known about the regional drainage, except that a major river followed a northwest course from Asyut and debouched at the eastern tip of the Qattara Depression (Fig. 1). In late Miocene time the Mediterranean Sea dried up and a river called the Eonile began forming which, because of the enormous drop in base level, cut a majestic canyon from the vicinity of the present Nile Delta to Aswan. In depth and width this valley was comparable to the Grand Canyon of the Colorado in the United States, but the Eonile canyon was four times longer.

Early Pliocene time (about 5 million to 3 million years ago) was marked by refilling of the Mediterranean Sea; the Eonile canyon became a long estuary that filled with marine sediments to about one-third of its depth as far south as Aswan. Late Pliocene (about 3 million to 2 million years ago) was marked by a cool, wet climate in which the "Paleonile" formed and converted the estuary into a channel. Aggradation by the Paleonile system eventually filled up the previous canyon (according to Said, about 20 percent of the fluvial sediments in the Nile Valley were deposited by this Pliocene river system). In the early Pleistocene aridity set in, Egypt became a desert, and, according to Said (*20*), the Paleonile stopped flowing. Toward the end of early Pleistocene (about 800,000 years ago) a relatively short-lived but very energetic river, the "Protonile," formed; it deposited distinctive cobbles and gravels [the Idfu gravels; "Early Nile Gravels" of Giegengack (*24*)] in the Nile Valley, in a course parallel to the modern Nile but 10 to 15 km to the west and at elevations as much as 100 m above the modern floodplain. The sources of this river are not certain, but are considered to have been the same as those of the Paleonile.

Stream captures in the Ethiopian highlands led to the breaking through of the "Prenile" into Egypt, and this highly energetic river cut a new course separate from that of the older Niles, but essentially within the confines of the present Nile Valley (Fig. 3d). The Prenile was a vigorous river that deposited, for the first time in lower Egypt, sediments that contain epidote and pyroxene. These minerals could only have been derived from streams flowing from east-central African sources (*25*). The relative percentages of these two minerals in Prenile sediments differ only slightly from those in sediments of the modern Nile. Enlargement of the Nile drainage basin continued with successive capture by the Prenile of Wadi Atbara and the Blue Nile (Fig. 1). The Prenile, however, died out before the Abassia pluvial, an episode of lesser aridity that is marked by gravels containing Acheulean artifacts (200,000 years ±100,000 years old) and that profoundly affected the Arbain region to the west.

The Prenile was followed by the "Neonile," a weak successor whose early history is marked by a long interval of recession and minor flow. About 10,000 years ago the Neonile assumed a character very much like that of the modern Nile, probably owing to its capture of the White Nile (Fig. 1). This event resulted in the almost total integration of what is

Fig. 2. Characteristic features of the Arbain Desert and their tonal responses to the shuttle imaging radar. (a) Wind-pitted and -fluted, low outcrops and mostly 0.3-m talus blocks of Nubian sandstone partly mantled by drift sand: intermediate mottled (*im*) (Table 1). (b) Bare, decimeter-scale, wind-fluted limestone at the edge of the Limestone Plateau a few kilometers north of area VI (Fig. 9): bright (*b*). (c) Uninhabited oasis of Bir Kiseiba, where the unusually shallow, about 50-cm-deep, water table supports date palms, dom palms, and grass hummocks: intermediate mottled (*im*) with very bright spots. (d) Compound barchanoid dune, estimated to be about 15 m high, with multiple slip faces: dune sand gives mostly very dark response, with scattered very bright spots where radar energy may be specularly reflected from slip faces or backscattered from shallowly buried interdune outcrops; entire dune trains thus give dark mottled (*dm*) response. (e) One of the Two Hills, conical outliers of the Kiseiba scarp, with rubbly talus slopes: very bright (*vb*). (f) Lake beds (area VI, Fig. 9): dark (*d*). (g) Valley fill (area I, Fig. 4): dark (*d*). (h) Sand plain near Bir Abu Hussein (area V, Fig. 8): dark mottled (*dm*).

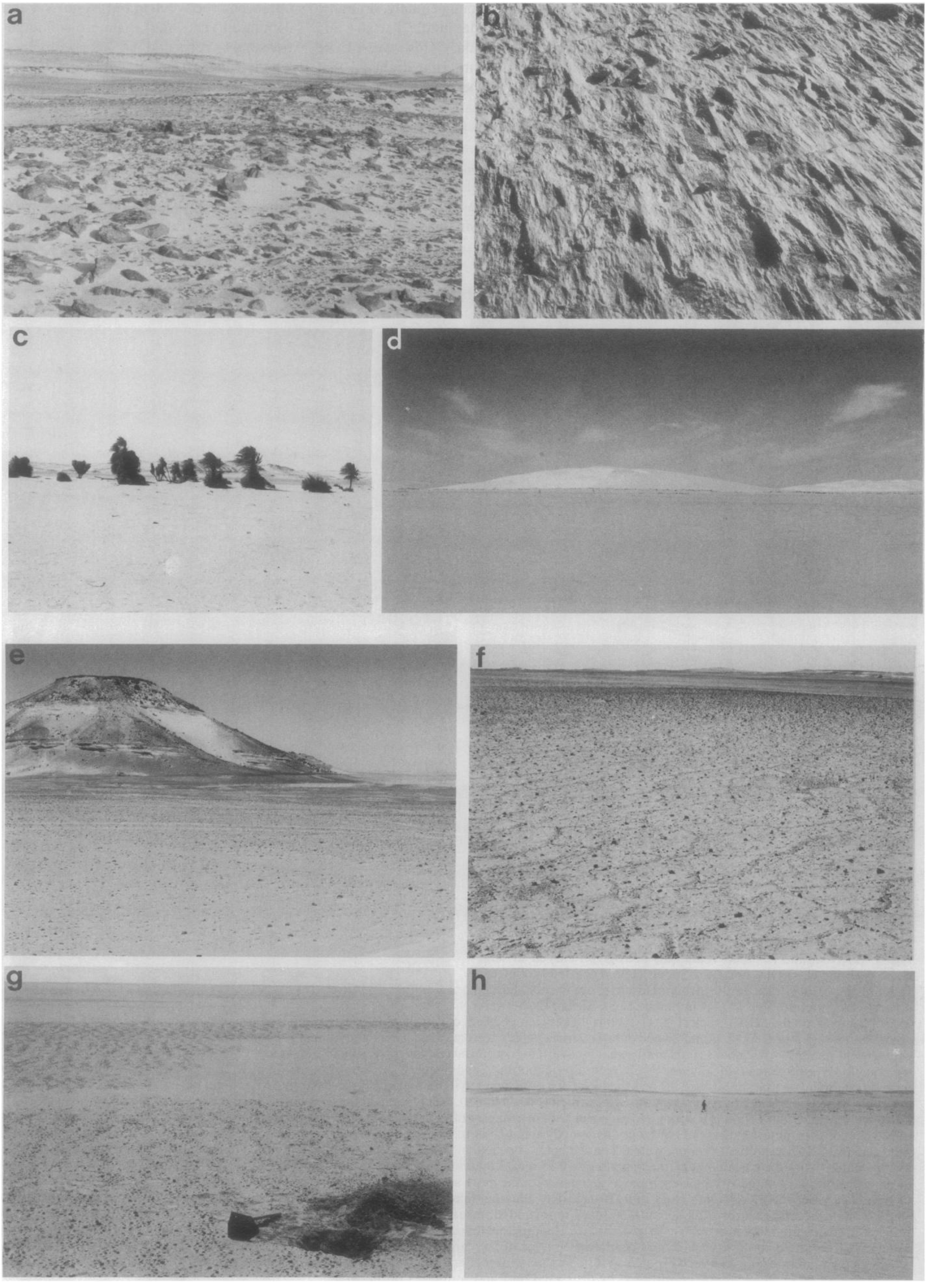
a
b
c
d
e
f
g
h

now the longest river in the world, extending from the Mediterranean to Lake Victoria. The destinations of such major equatorial African water sources as Wadi Atbara, the Blue Nile, and the White Nile, before their capture by the Egyptian Nile, remains a mystery whose solution, perhaps, lies in the paleodrainage of the Arbain Desert as revealed by SIR-A.

West of Sudan in the central Sahara another great drainage basin was developing and undergoing equally dramatic changes through the middle Tertiary and Quaternary periods. This was Lake Chad, a basin of internal drainage that several times in the past was about the size of the Caspian Sea (*26*). Several highstands of the lake are recognized (the most recent at about 5500 years ago). According to Servant and Servant-Vildary (*27*), the oldest fossils identified from borings in the lake are middle Miocene, and the basin may be as old as Oligocene (between about 38 million and 24 million years ago). Numerous fluctuations are recorded in its sediments, which range from fluviatile clastics to cool-water diatomites. The lake was cut off from any outlet to the sea between 5 million and 4 million years ago (early Pliocene). Calcareous sediments appeared between 3 million and about 2 million years ago, along with intercalations of eolian sand that coincide with the same general onset of aridity, near

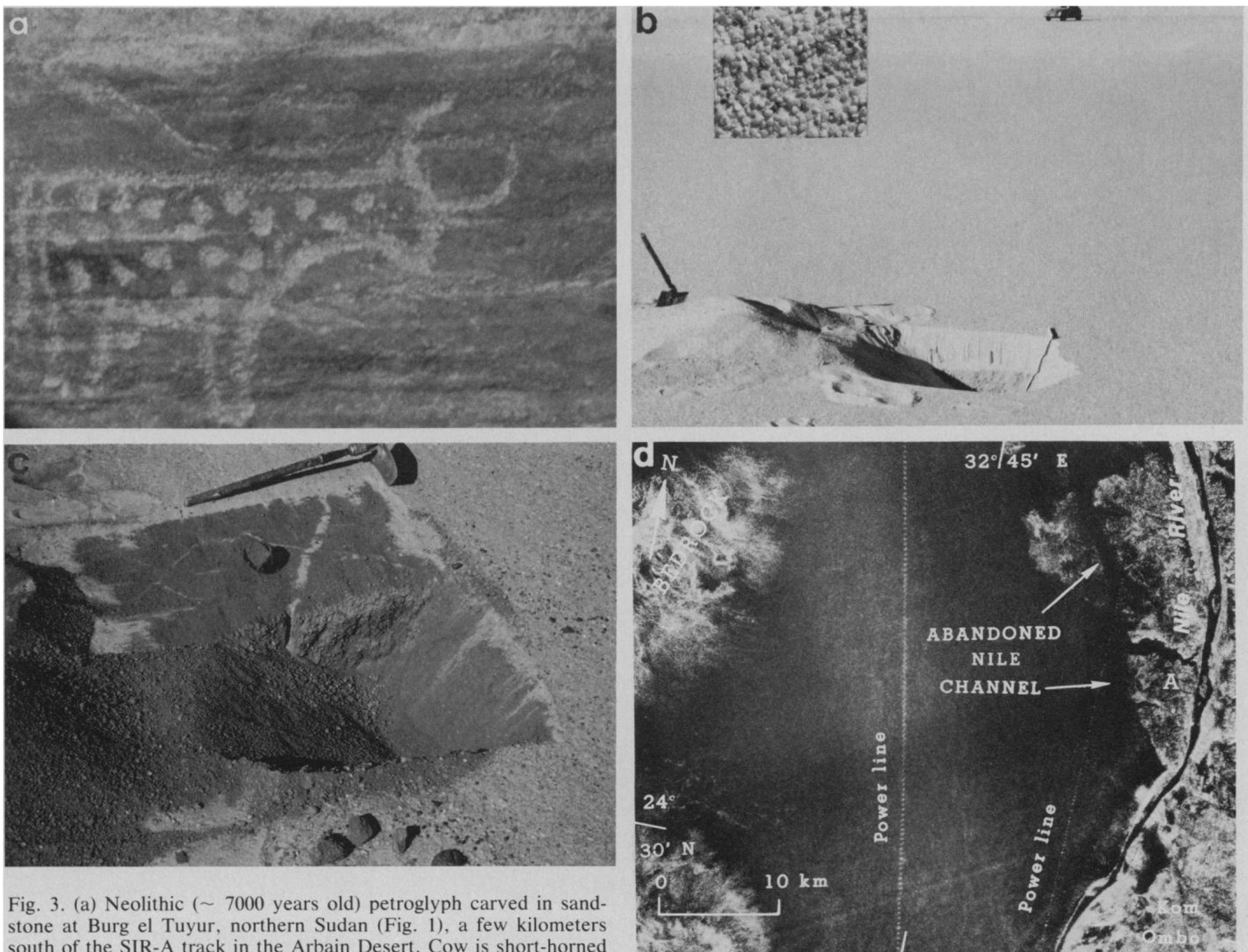

Fig. 3. (a) Neolithic (~ 7000 years old) petroglyph carved in sandstone at Burg el Tuyur, northern Sudan (Fig. 1), a few kilometers south of the SIR-A track in the Arbain Desert. Cow is short-horned domesticated variety (*49*). (b) Pit in Selima Sand Sheet (*12*) between areas III and IV on the SIR-A track (Fig. 1). At this locality about 20 cm of soft, laminated, unweathered eolian sand [color 7.5 YR on Munsell soil color chart; stage 0 of C.V.H. (unpublished data)] overlies pebbly to coarse red sandy alluvium. The Sand Sheet consists of bimodal, very fine to coarse sand (modes ~ 1.2 and ~ 0.08 mm) typically overlain by a surface layer of very coarse sand and granules (coarse mode ~ 1.0 mm). The lag granule layer (inset) is typically one grain thick throughout the Sand Sheet. Calculations based on measured electrical properties of samples from this pit indicate that the surface lag and the loose dry sand beneath it are essentially transparent to the radar beam (see text) (Table 2). (c) Pit in Selima Sand Sheet south of area III on the SIR-A track (Figs. 1 and 6). Here the Sand Sheet is only 2 cm thick over pebbly alluvium at least 270 cm deep. The alluvium contains a strong red paleosol (2.5 YR; stage 4 of C.V.H.) with very coarse prismatic structure. Alluvium sampled at 260 to 270 cm consists almost entirely of quartz grains, mostly subangular to subrounded (about 15 percent are rounded), suggesting its origin as drift sand reworked by intermittent running water. The red color is pedogenic, due to a coating of iron oxide. Unlike the overlying bimodal sand, the alluvium at 260 to 270 cm is unimodal (mean grain size 0.35 mm, a medium sand), moderately sorted, coarse-skewed, and very leptokurtic. Some of the oldest artifacts in the Arbain Desert are associated with the more strongly developed alluvial soils such as those in this pit. (d) SIR-A image of Nile Valley between Kom Ombo and Idfu. Broad, dry, alluvium-filled valley is dark mottled on radar, suggesting the presence of both flat, smooth alluvial surfaces at or near the surface (dark tone) and surfaces with sufficient roughness to backscatter at the SIR-A wavelength; the rougher surfaces are shown as diffuse bright patches trending northwest in the floodplain, and may consist of gravel bars. Power lines carry electricity from the dam at Aswan. Note abandoned courses of the earlier Nile River and its tributaries incised in bedrock or gravel terraces, which give an intermediate mottled response at *A*; compare with modern Nile River in narrow, bright, vegetated (irrigated) valley. Abandoned earlier Nile River channel is largely obscured by drift sand on Landsat images of this area.

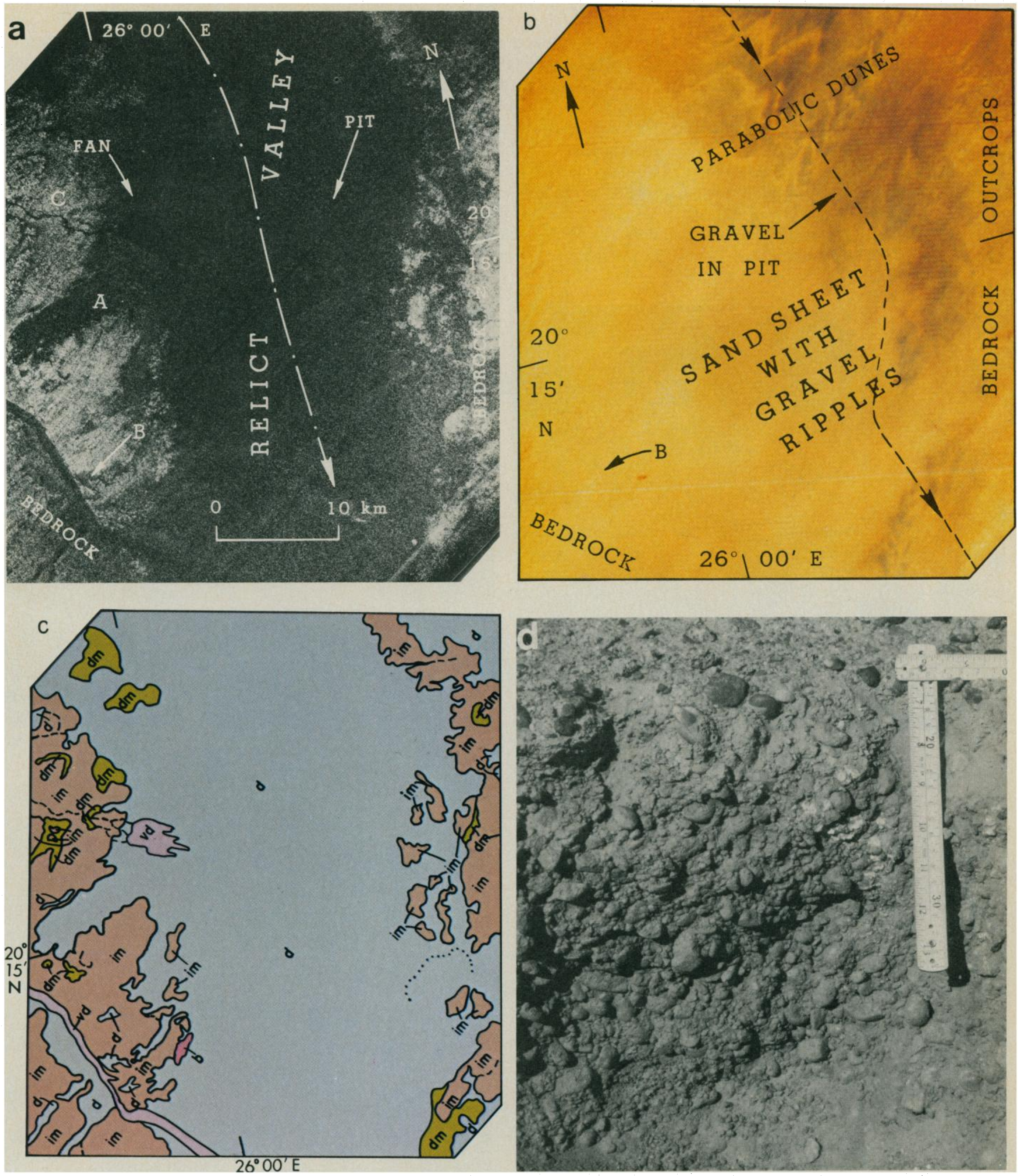

Fig. 4. Area I south of the Gilf Kebir plateau, southwest Egypt, and north of Merga Oasis, northwest Sudan (Fig. 1); (a) to (c) are at the same scale. Comparison of (a) SIR-A and (b) Landsat images indicates that radar has penetrated the veneer of eolian drift sand [yellow in (b)] and parabolic dunes to reveal large and small buried stream valleys. (c) Map based on radar image shows 25-km-wide dark trunk valley with stubby tributary valley at *A* on radar image, surrounded by low outcrops that give an intermediate mottled (*im*) response. Narrow, underfit tributaries at *B* and *C* on radar image are channels incised in bedrock, now filled with windblown sand and silt; the smooth surfaces appear as very dark (*vd*) linear features in (c). One of these wadi systems (at *C* on radar image) built a fan on the floor of the trunk valley, probably during Quaternary flashflooding. The incised wadi at *B* is also partly visible beneath sand cover on Landsat. Trunk valley is interpreted as part of a Tertiary (?) regional south-flowing drainage system [dashed line in (a)], possibly connected to drainage from Gilf Kebir (*13*, *14*, *17*). Compare breadth of this relict, buried valley with that of the Nile Valley at the same scale (Fig. 3d). Pit along 1982 traverse by C.V.H. and M.J.G. [dashed line in (b)] contains stream-rounded pebbles and cobbles of stage 2 or 3 alluvial soil (C.V.H., unpublished data) with vesicular horizon and irregular calcic patches [ground photo (d)]. Pit is in otherwise nearly featureless sand plain marked by low sandstone outcrops and patches of wind-rippled and ventifacted gravels (Fig. 2g).

the beginning of the Pleistocene, that was experienced in Egypt.

Knowledge of the geologic history of the divide between the Nile basin and the Chad basin is extremely poor. To the south, structural warping of the Gebel Marra basement rocks (Fig. 1) formed a dome some 500 m high with a 140-km-long superposed volcanic complex that began in the Miocene and continues with solfataric activity to the present; this major geologic edifice has undoubtedly caused major as well as minor diversions of the regional drainage systems. Adamson and Williams (*28*) document the capture of the western end of Wadi Howar (*29*), whereby 60,000 km^2 of catchment area of the Nile basin was diverted to the Chad basin. Similarly, parts of the Blue Nile and Wadi Atbara show remarkable recurvature, as if they were forced westward as they found their way around shield volcanoes, structural uplifts, and volcanic piles emplaced during the Tertiary. The Nile itself makes a great bend in the middle Sudan around the Bayuda Volcanics, which lie on a northeast trending, trans–North African rift zone that extends from Mount Cameroon (south of the map area on the Atlantic Ocean) through the Gebel Marra complex to the Bayuda volcanic field (Fig. 1). The Gebel Marra basaltic-trachytic stratovolcano complex lies at the intersection of this structural trend with a northwesterly oriented line of structures and volcanics that passes through the Tibesti complex and the Gebel Haruj, the Gebel es Soda volcanics, and the

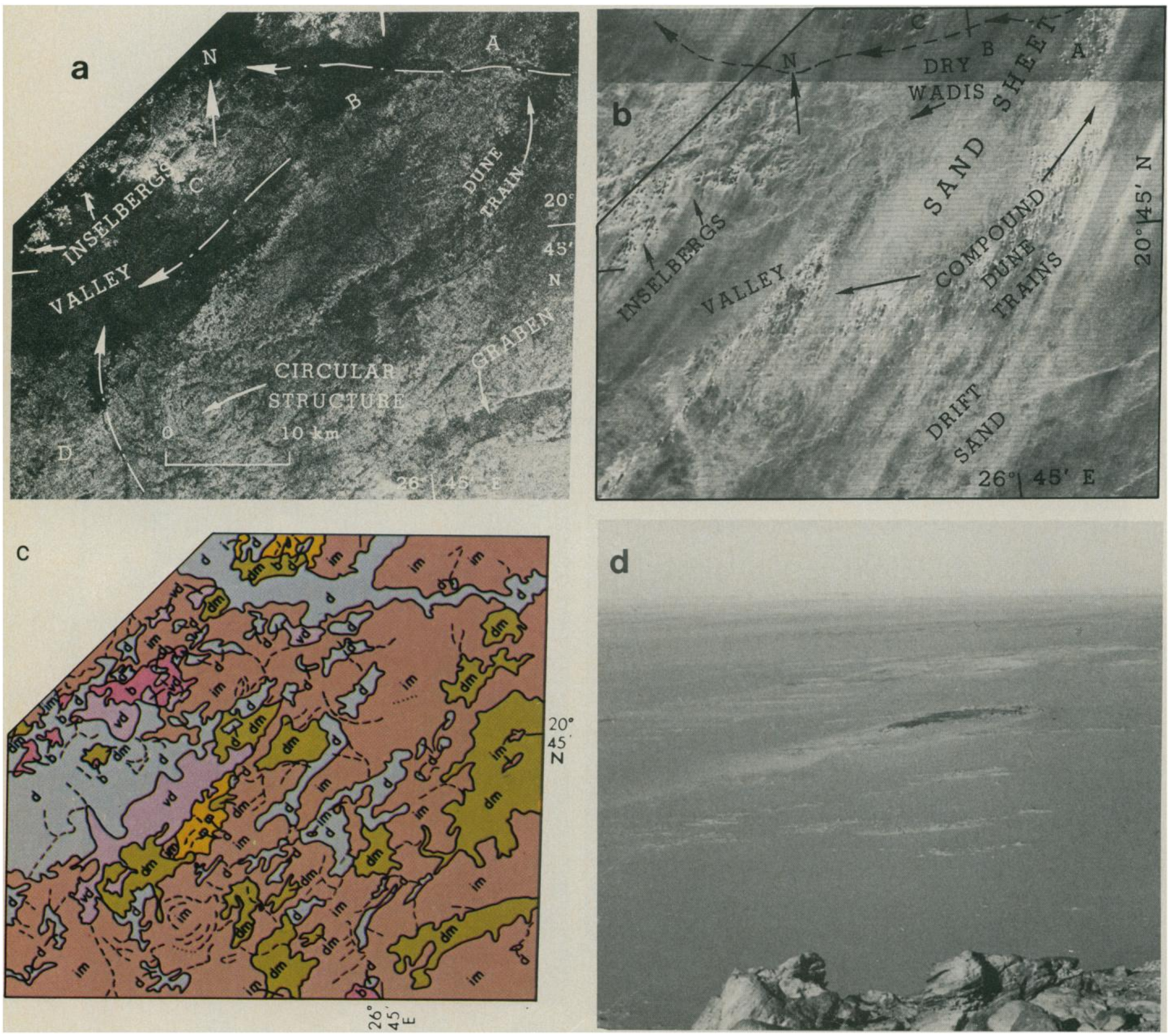

Fig. 5. Area II, west of Burg el Tuyur, northwest Sudan (Fig. 1); (a) to (c) are at the same scale. (a) Radar image shows fault troughs (graben), multiringed circular features that resemble structures identified as igneous intrusives in the Eastern Desert (*57*), and numerous well-integrated but dry wadi systems. These features are mostly obscured beneath the Selima Sand Sheet and trains of barchanoid dunes (point *A*) and drift sand on the Landsat image at the same scale (b). Only where the sand is exceptionally thick (dunes about 10 to 15 m high, as shown in Fig. 2d) is the radar signal unable to penetrate to a reflecting substrate. Very dark irregular bulbous feature on the radar image at *D* represents a former lake. Wadis apparently drained northward and westward into the trunk valley possibly tributary to the large south-flowing Tertiary (?) system in area I (Fig. 4). This area is a transition zone between the relict fluvial topography still visible in the western part of the Arbain Desert and the present-day eolian takeover in the central part marked by the Selima Sand Sheet and associated sand dunes. The edge of the sand veneer is approximately at point *B*. The ground photo (d) taken from point *C* on the ground traverse (dashed line) shows an inselberg in the foreground [bright on the radar image and on the map in (c)] overlooking a broad relict fluvial valley (dark on radar) in which low outcrops of sandstone (mottled on radar) protrude above the valley fill.

Nefusa Uplift that lies just south of Tripoli (off the map, Fig. 1) on the Libyan coast (*30*). The evolution of the Gebel Marra and the even more imposing Tibesti volcanic complex, along with Gebel Uweinat at the intersection of Egypt, Libya, and Sudan (Fig. 1), must have had profound effects on the pre-Pleistocene regional drainage of the eastern Sahara.

Many earlier workers in the eastern Sahara speculated on former connections between the Chad and Nile drainage basins. On the basis of similarities between fish fauna in Lake Chad and the Nile River, it was suggested (*31*; *32*; *33*, pp. 157–159 and figure 10) that drainage from an ancestral Upper Nile was connected with that of Lake Chad. Such a connection would neatly solve the problem of what to do with the present Nile's older equatorial headwater tributaries prior to their successive capture from east to west during middle to late Pleistocene. Holmes (*33*, p. 159 and figure 10) suggested that drainage from Lake Chad may have reached the Upper Nile at Dongola via Wadi Howar (Fig. 1). This may be consistent with the known eastward extent of Lake Chad during the Quaternary pluvials, when the lake rose to elevations of at least 320 m (*26*; *34*, figure 1).

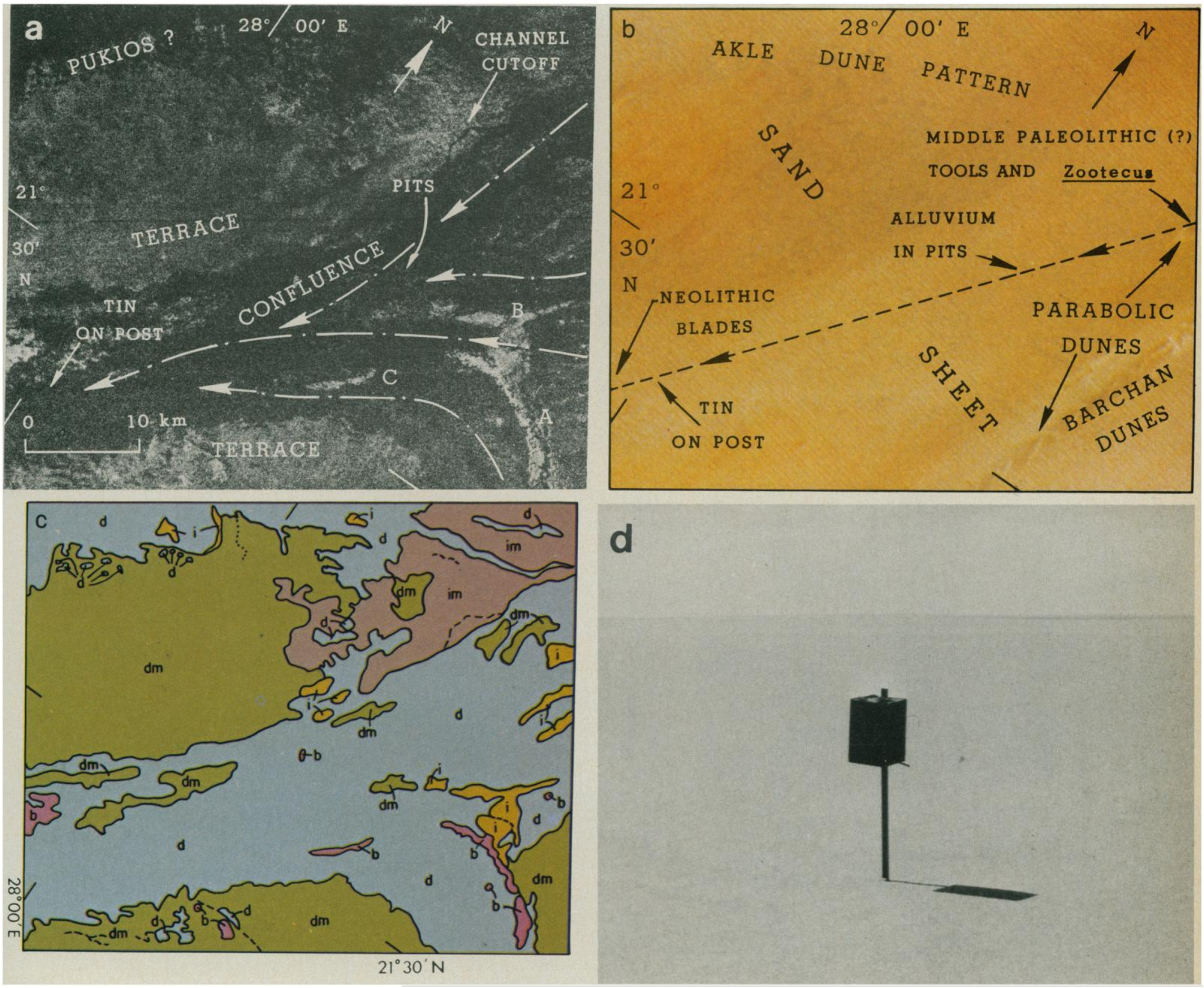

Fig. 6. Area III, central part of the Selima Sand Sheet, northwest Sudan (Fig. 1); (a) to (c) are at the same scale. (a) Radar image revealing confluence of several braided channels (dashed arrows) in a large trunk valley. Samples of alluvium from pits at depths of 28 to 33, 18 to 22, and 260 to 270 cm in the main valley are nearly 100 percent quartz grains. Flow in main valley was toward west. (b) Landsat image shows several overlapping eolian sand sheets with traces of aklé dune patterns (*51*) and a scattering of active barchans, but no trace of underlying fluvial topography. Comparison of the radar and Landsat images and the map (c) indicates a relation between the buried river banks and terraces, faint traces of parabolic dunes, and presence at certain localities of Stone Age human artifacts, ostrich shells, and shells of *Zootecus insularis*, a land snail indicative of formerly moist soil and vegetation (*77*, *78*). Some pits in the sand sheet in this vicinity reveal a strong paleosol in alluvium beneath a thin veneer of windblown sand. Irregular dark patches in the northwest part of the radar image are interpreted as former interdune basins. This area is less than 100 km north of Burg el Tuyur, where a petroglyph of a domesticated cow is estimated to be about 7000 years old (Fig. 3a). (d) Ground photo showing a marker tin (about 33 cm long) on a post used by the Sudan Defense Force (1934) to navigate across this now barren, essentially featureless, and extraordinarily flat sand plain on which no trace of former fluvial activity is seen.

Wadi Howar (*29*) is a dry stream course that extends eastward toward the Nile River across northern Sudan; it passes about 650 km south of the Gilf Kebir plateau and is about 200 km north of Gebel Marra. Wadi Howar marks the south boundary of the Arbain Desert (*2*). Major streams flowing from the southern Gilf highlands in middle to late Tertiary time may have reached Wadi Howar and thence discharged into the Upper Nile. Or Wadi Howar may have reversed its course once or more due to disturbances in the Gebel Marra area and may thus have flowed into Chad after receiving discharge from the former Gilf Kebir drainages and from the large west- and south-flowing, now defunct stream courses discovered by SIR-A. Some of these buried stream valleys in the Arbain Desert could be ancient connections to the troublesome Upper Nile tributaries. However, samples of alluvium dug from pits in these valleys are nearly 100 per-

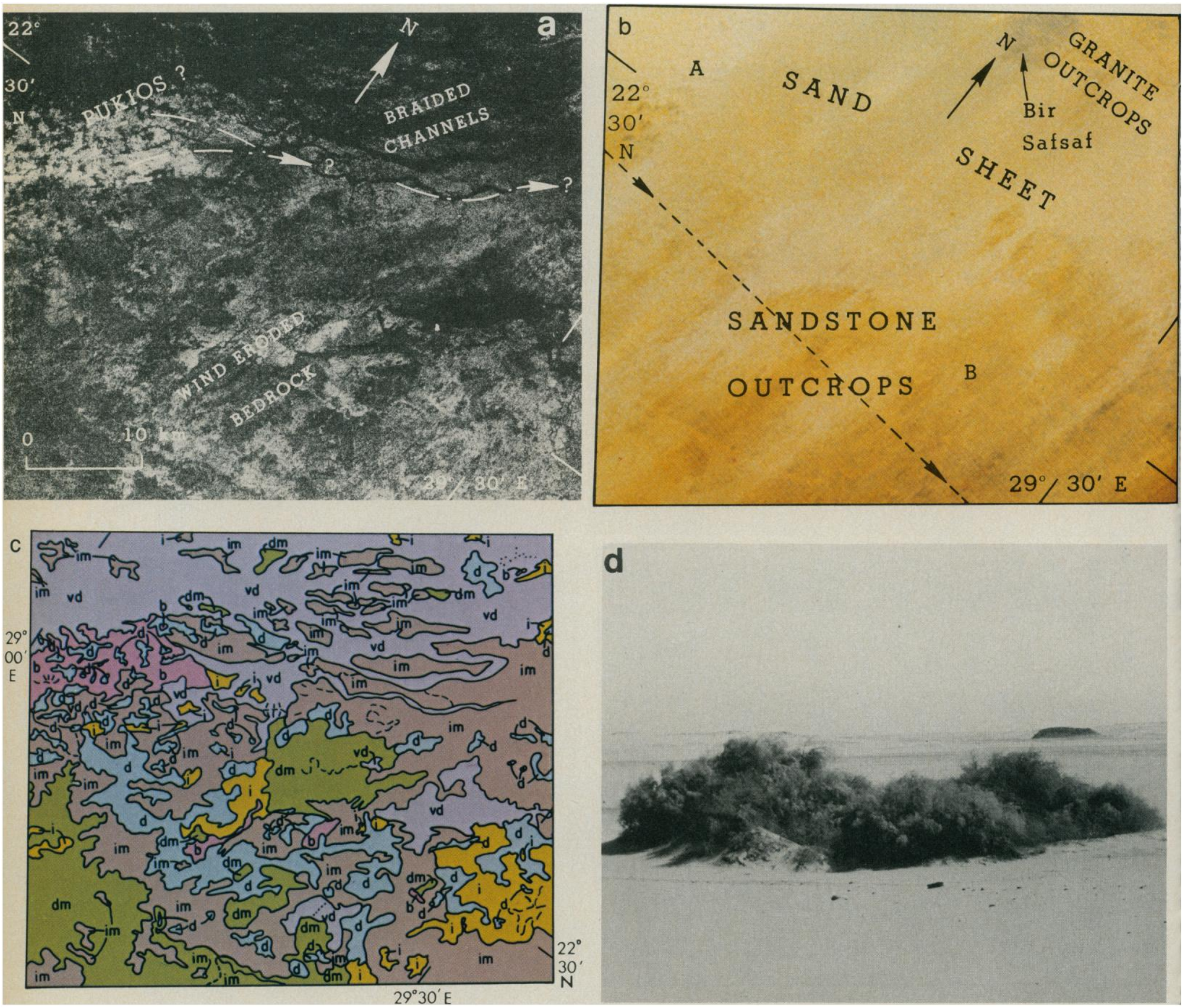

Fig. 7. Area IV, at eastern edge of the Selima Sand Sheet, southern Egypt (Fig. 1); (a) to (c) are at the same scale. (a) Radar image showing large braided relict stream courses concealed beneath the Sand Sheet on the Landsat image (b). Bir Safsaf is located in the middle of the old stream courses. Very dark areas at *A* in (a) correspond to sand-filled former interdune basins in (b); some of the basins may have been episodically or seasonally flooded when water flowed on the adjacent floodplain. Direction of former streamflow is uncertain but appears to be eastward [dashed lines in (a)], suggesting a drainage divide between this area and area III (Fig. 6). Bedrock areas to the south are dark on the Landsat image; their radar responses range from bright (rough outcrops) to very dark, as at *B* (outcrops mantled by eolian sand but to depths from centimeters to 1 m or more). Complex pattern of bedrock responses on the map of radar units (c) reflects partly buried structures and different surface roughness characteristics. Radar and Landsat images both show a strong eolian erosion "grain" parallel to the dominant north wind. A probe of the Sand Sheet in the buried channels found moisture at a depth of 3 m. "Tarfa" (*Tamarisk* sp.) still grow in numerous localities aligned with the buried channels. (d) Ground photo showing an ancient abandoned well surrounded by tamarisk bushes (clump about 5 m in diameter) in this depression. According to Ball (*39*), the water table in this area dropped in historic time as water was drawn from wells in the Kharga Depression about 300 km to the north.

cent quartz grains and lack the heavy mineral grains, mainly epidote and pyroxenes, that would be diagnostic of exotic source rock localities. The samples were obtained mostly from shallow depths of a few tens of centimeters; deeper sampling is planned for the next field season.

The present regional slope of the land surface in the southwest corner of Egypt is, according to existing maps, generally northward, but the detailed topography of the region is poorly known and essentially unmapped. Capture of some of the wadis of the Gilf Kebir plateau by the south-flowing Eight Bells system and by other streams that eroded headward into the west side of the Gilf during less arid episodes (*14, 17*) implies former steeper gradients to the south and west than to the north in these areas. Relief maps of North Africa such as that by Raisz (*35*) and Fig. 1 suggest that, if the Gilf Kebir plateau were indeed once a major divide separating east- and north-flowing from south-flowing drainages in the Arbain Desert, the latter streams might have eventually discharged into the Bodélé Depression in the Borkou region of northern Chad, perhaps by way of the Mourdi Valley, without ever having been joined with Wadi Howar. Such drainage directions would have to predate uplifts of the Uweinat and Tibesti complexes and associated volcanism that surely have disturbed the regional gradients in the eastern Sahara.

Methods and major results of radar mapping. The radar swath from the vicinity of the Mourdi Valley in northeast Chad across northwest Sudan to Kom Ombo, just north of Aswan on the Nile, was studied, but only six areas, each about 40 by 50 km (areas I to VI in Fig. 1), were analyzed and mapped in detail. The choices were dictated by time constraints; by the location of our ground tracks during expeditions in 1978, 1980, and 1982; and by the availability of suitable ground pictures and samples illustrating the various types of radar units that we can recognize. As far as possible, each of the six areas mapped was chosen on the basis of the presence of previously unknown or hard-to-detect geological features, the delineation of which depends on the ability of the SIR-A radar to "look through" the almost continuous eolian blanket now covering this hyperarid region.

The principles used in geologic mapping of the moon and other terrestrial planets were applied to the radar data because of their rigor and success in deciphering strange, previously unexplored terrains (*36, 37*). The radar units that can be mapped in a coherent and logical fashion are identified in Table 1; many are illustrated by ground photographs along the SIR-A track (Figs. 2 and 4d through 9d). The units are ordered from the brightest to the darkest—

Table 1. SIR-A map units and explanation (see Figs. 4c to 9c).

Description	Interpretation
Very bright [*vb*]	
Small linear streaks and circular or elliptical spots with highest radar response. Mostly less than 0.5 km in size. Features too small to map are included in bright or mottled units.	Rubbly scarps and isolated, steep-sided, conical hills partly covered with rough, wind-eroded talus fragments larger than 8 cm (Fig. 2e); calcareous tufa mounds that were basal artesian springs, but now stand isolated from retreating cliffs; patches of vegetation, mostly tamarisk mounds and minor palm tree oases (Fig. 2c). All are of positive relief features.
Bright [*b*]	
Extensive tracts of almost uniformly bright terrain with sharp curvilinear and rectilinear boundaries with darker terrain. Frequently encloses darker surfaces in elliptical to irregular envelopes that resemble an onionskin pattern. Also forms long, sinuous, semispotted zones or highly irregular, isolated patches that are coincident with known scarps (Figs. 2a, 5, 8, and 9).	Mostly bare, wind-grooved, and pitted bedrock: limestones and shales of lower Tertiary age at the eastern end of the SIR-A track (Figs. 2b, 8, and 9). Nubian sandstone and possibly older rocks to the west (Figs. 4 to 7).
Intermediate [*i*]	
Small irregular to elongate patches of medium but fairly uniform radar response, mostly in areas mantled by the Selima Sand Sheet and along the edges of or within large dark areas that have the form of broad river valleys.	Low wind-roughened bedrock outcrops, low rubbly scarps along riverbanks, and possible large gravel bars within river valleys, mostly bare of sand or thinly buried.
Intermediate mottled [*im*]	
Areas of mostly intermediate radar response but containing numerous darker and lighter patches too small to map. This most extensive radar unit locally forms large irregular patches and elongate streamlined riverbar-like patches.	Low outcrops, gravel river terraces, or bars thinly covered by windblown sand. Locally enclosed, circular to elliptical dark areas represent sand- and alluvium-filled structural or topographic depressions.
Dark [*d*]	
Surfaces uniformly low in radar response are second most extensive radar unit. Largest expanses are in broad, relatively featureless valleys 15 to 25 km wide; also occurs in smaller, sinuous channels that appear to be underfit tributaries to the large valleys.	Sand and pebble alluvium in dry river channels, on floodplains, and in small structural and topographic depressions; some depressions have rectilinear outlines and may be man-modified.
Dark mottled [*dm*]	
Elongate curved streaks and irregular patches of very dark reflectivity containing numerous small bright spots.	Areas of thick sand or alluvium except for scattered spots of near-surface or surface radar-rough terrain too small to map. Also trains of large dunes whose sand is too thick for SIR-A to penetrate (see text). Thick dunes are generally extremely radar-smooth (very dark), but slip faces may give a very bright, specular response (Figs. 2d and 5).
Very dark [*vd*]	
Small sinuous, linear, and irregular patches of extremely low radar response. Commonly occurs in dendritic and braided patterns, some ending in fanlike patterns superimposed on the dark unit; these occur mostly toward western edge of SIR-A track (Fig. 4).	Mostly fine-grained sand and silt deposits of Quaternary intermittent or ephemeral streams (wadis) that carried runoff into the low-lying valleys from headwater regions outside the mapped areas. Some may be relatively recent cloudburst and flash flood deposits (Fig. 9d), but very dark response indicates extremely smooth surfaces without coarse gravels (see text).

that is, from the areas with the greatest radar return to those with the least return. No age connotation is intended by the ordering of units. The maps based on these radar units (Figs. 4c through 9c) are therefore, in a strict sense, terrain maps rather than geologic maps. Many of these units can be identified from past ground observations, from pits that have been dug at many localities, from geologic maps of parts of the region (*38*), and from photographs, only a few of which can be shown here. The origins of other units are less certain, and definitive interpretations will have to await the results of future field investigations guided by both the SIR-A data in hand and the data anticipated from SIR-B in 1984.

The most striking result of the experiment in the eastern Sahara is that the SIR-A pictures, even with only preliminary processing (Figs. 4a to 9a), and the radar terrain maps made from them (Figs. 4c to 9c) show unambiguously the

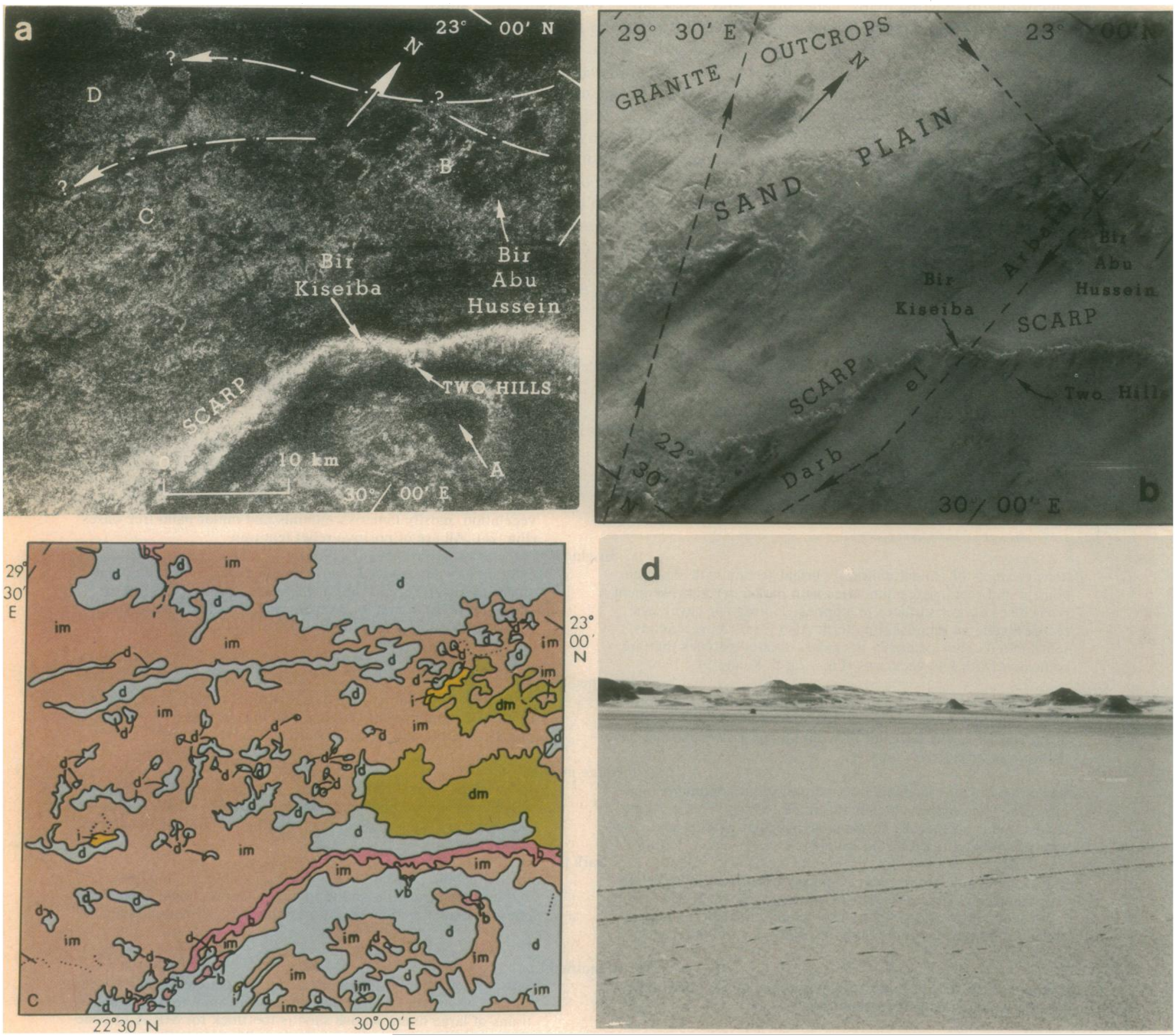

Fig. 8. Area V along the Darb el Arbain between Bir Abu Hussein and El Shab (Fig. 1); (a) to (c) are at the same scale. (a) Radar image showing rough broken Kiseiba scarp (*38*) as a prominent bright feature and adjacent sand-covered plain as mostly dark and intermediate mottled zones [*d* and *im* in (c)]. Several distinct zones are typically surrounded by intermediate mottled outlines, suggesting rubbly, rough boundaries. Pits in the largest of these dark zones, at *A*, contain alluvium (C.V.H., unpublished data). Other dark zones, at *B*, *C*, and *D*, near Bir Abu Hussein, are semirectangular and may have been modified by man. The sand plain northwest of Bir Abu Hussein is shown in Fig. 2h. Relict wadis nearby are now obscured by the sand plain (here known as the Atmur el Kibeish) as shown in (b). Two Hills are prominent conical outliers (Fig. 2e) that are barely visible on Landsat but very bright on the radar image at the same scale. Some bright spots along the scarp may be spring mounds, which cannot be distinguished on these images from conical hills that are erosional remnants of old stream divides (*13*, *14*). The (d) ground photo showing broken topography of the Kiseiba scarp in the background (bright on radar) and smooth sand plain in the foreground (dark on radar). Vegetation is presently limited to oases such as Bir Kiseiba (Fig. 2b).

presence of major subjacent features that are not detectable even on specially processed Landsat pictures at the same scale (Figs. 4b to 9b) produced by techniques summarized by Chavez *et al.* (*16*). Neither can many of these features be seen on the ground photographs (Figs. 4d to 9d). The dramatically portrayed subjacent features are interpreted as segments of defunct major river systems, some of which have floodplains as wide as or wider than that of the Nile Valley far to the east (compare Fig. 4a with Fig. 3d). The broad trunk valleys have only a few equal broad tributary valleys, and these appear stubby and beveled, as if truncated by long intervals of wind abrasion and deflation. These stubby broad valleys, and the much smaller wadi networks superimposed on them, have junction angles with the trunk streams (the familiar rule of V's) that indicate westward, northward, and southward drainage. These former streamflow directions are not consistent with the major buried waterways ever having been connected with the present Egyptian Nile drainage. We suggest that the large valleys are relics of Tertiary systems that drained the eastern Sahara long before the onset of general aridity in the early Quaternary and long before the integration of the Nile.

Ancient Tertiary rivers that flowed in the directions indicated by the radar pictures (dashed lines on Figs. 4a to 8a) are inconsistent with the present regional trend of the water table in Egypt, known from well data since at least 1927 (*39*) to slope gradually from high ground in the southwest northward toward the Qattara Depression and the delta of the modern Nile (Fig. 1). This need not, however, weaken the case, supported by ground explorations and Landsat analyses, for the former existence of major southward- and eastward-flowing drainage systems that issued from the highlands of the Gilf Kebir (*14, 17*). The SIR-A discoveries help corroborate our earlier interpretation of the Gilf Kebir plateau as a major pre-Pleistocene divide in the eastern Sahara and our conclusion that the pediplane of the Arbain Desert was carved by large, highly energetic streams during the interval between the retreat of the Eocene sea and the beginning of Quaternary aridity. The distribution of ancient divides, now reduced to conical hills (*13, 14*), ventifacted alluvial gravels, and the topographically controlled courses that many dune trains follow along apparent old stream valleys, was beginning to point strongly in this direction even before the availability of the SIR-A data. Detailed regional reconstructions of these previously unknown drainage systems await more extensive radar coverage.

Underfit tributaries and narrow channels within the partly to completely buried floodplains of the master streams on the radar images (Figs. 4a and 5a), indicate that parts of these large watercourses were used time and again, probably by intermittent running water during Quaternary pluvial episodes. The dashed lines and bulbous or curvilinear segments of dark and very dark radar response (Figs. 5c and 8c) that mark the traces of some of the smaller channels are reminiscent of the billabongs (dry season, watered cutoffs on low-gradient streams) characteristic of the relict drainage of semiarid to arid central Australia (*40*). The SIR-A pictures thus reveal a series of palimpsest drainages in the Arbain Desert that are probably related to several episodes of fluvial activity, some perhaps as old as Oligocene but others as recent as the Quaternary pluvials that coincide with human occupations.

Geoarcheological work in the Western Desert indicates three major periods of human occupation in this region before early prehistoric time (*2, 9, 12, 41–46*). In general, the earliest late Acheulean artifacts (possibly of *Homo erectus*) are associated with ancient river deposits and later, as the climate deteriorated, with tufa mounds (C.V.H., unpublished data). The tufa mounds were spring sites that about 200,000 ± 100,000 years ago were basal to retreating cliffs that contained artesian aquifers (*47*). Middle Paleolithic occupation (possibly by *Homo sapiens neanderthalensis*) appears to be associated with both alluvial deposits and the dunes that since early Pleistocene had begun to overrun parts of the Western Desert. Remnant populations of pastoral nomads in the Sahara still use interdune flats and riverine environments for temporary habitation during wet cycles (*48, 49*). Neolithic artifacts in the Arbain Desert (left by *Homo sapiens sapiens*) are mostly limited to playa and eolian deposits, except where they have apparently been lowered by deflation to older alluvial surfaces. This relation attests to the increasing severity of the environment as Egypt moved closer in time to its present hyperarid condition.

Comparison of the simulated true-color Landsat image (*50*) and the radar image of area III (Fig. 6, a and b) illustrates the relation between places where artifacts and shells are found in and on the Selima Sand Sheet and the underlying fluvial landscape revealed by SIR-A. The 1982 traverse by C.V.H. and M.J.G. across this area (dashed line in Fig. 6b), unbeknownst to them, followed a concealed valley that was formerly the confluence of several stream channels flowing from the north, east, and south (Fig. 6, a and c). No trace of this valley or of its numerous wadi channels was apparent on the Landsat image or in ground view (Fig. 6, b and d). Only random test pits placed during the past decade revealed alluvium below the windblown sand sheet (*12*). Comparison of the localities where artifacts and shells were found (Fig. 6b) with the pattern of buried channels and riverbanks (Fig. 6, a and c) suggests that these remains are meaningfully rather than randomly distributed. The artifacts found here include Middle Paleolithic tools, some reworked by Neolithic people, as well as Neolithic tools. For Middle Paleolithic people, the old riverbanks and terraces would have offered sites near probable seasonal sources of running water in the wadis and grassy shelter in nearby interdune flats, whose traces can be seen on the Landsat and radar images (Fig. 6, a and b).

Whereas the radar pictures show an ancient topography dominated by fluvial features, specially computer-processed Landsat images (*15*) best show the present surficial geologic units, which consist mostly of several distinct types of eolian deposits (*51*). False-color Landsat images indicate that the Selima Sand Sheet is not a single blanket of eolian sand over alluvium, but is built up of successive "waves" of overlapping sand, mostly in the form of featureless drifts and wind-truncated remnants of massed barchanoid dunes. Overriding all these are trains of actively migrating barchanoid dunes, which represent the most recent wave of sand invasion, probably from the Great Sand Sea to the north (Fig. 1). Several areas (Figs. 4b and 6b) show traces of chevron-shaped parabolic dunes that are apparently wind-truncated, for, unlike the active barchans, the parabolic dunes are not obvious in ground view. Similar dunes fixed by vegetation cover large areas in the more humid southern parts of the Sudan (*52*). Parabolic dunes typically form from erosional blowouts of vegetated sand sheet deposits in semiarid deserts. We interpret the traces of parabolic dunes in the Arbain Desert (Figs. 4b and 6b) as relics of earlier, less arid Quaternary climatic episodes, when the savanna extended northward into the Arbain region and the sand sheet surface was at least partly stabilized by vegetation. This was suggested independently by Haynes (*12*), who found a succession of sand sheet deposits, separated by paleosols, between Bir Tarfawi and Burg el Tuyur.

Another observation from SIR-A is the presence of dark and bright patches near the "radar rivers" (Figs. 6a, 7a, and 8a). The bright spots are typically surrounded by radar-dark terrain, whereas on Landsat images corresponding spots are dark and the surrounding terrain is bright (Figs. 6b, 7b, and 8b). The pattern is reminiscent of the ground water–skimming, interdune fields of pre-Hispanic coastal Peru (*53*), the only other desert with an aridity index comparable to that of the Arbain Desert (*54*). The pattern also resembles the network (aklé) pattern of dune ridges with fully enclosed interdune basins common to much of the

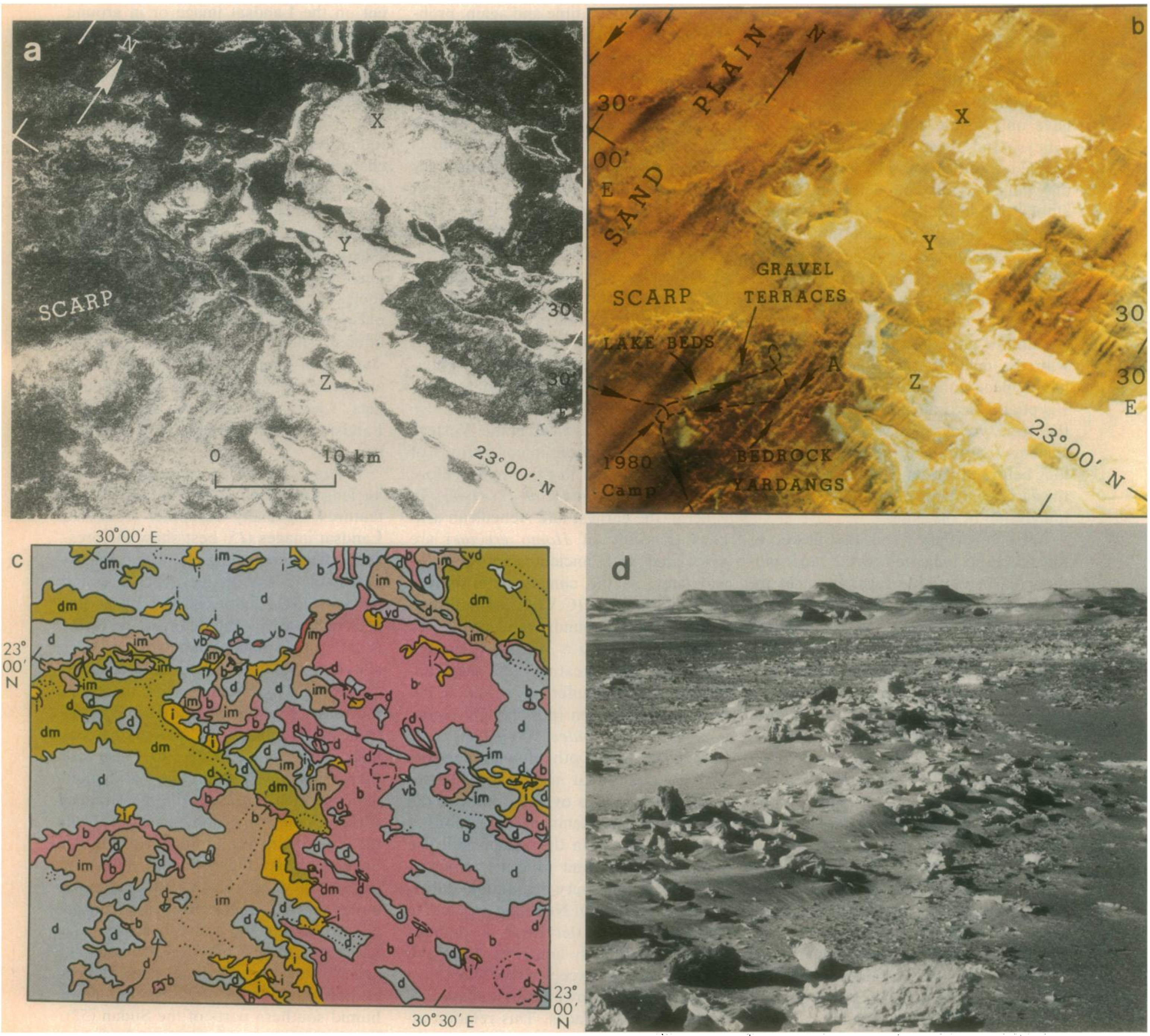

Fig. 9. Area VI at edge of Limestone Plateau east of Bir Kiseiba (Fig. 1); (a) to (c) are at the same scale. Radar image (a) shows large areas of rough bedrock on the Limestone Plateau (bright and very bright zones such as at *X*, *Y*, and *Z*), which are partly veneered by windblown drift sand (yellow) on Landsat image (b). The uppermost unit is the Dungul Formation of Eocene age, a nummulitic limestone that is highly reflective in the radar pictures even where buried by sand. Pits dug at locality *X* in September 1982 revealed a radar-rough surface of limestone (Dungul Formation) beneath 1.1 m of sand and colluvium. The Dungul Formation overlies the Garra Formation of lower Eocene to upper Paleocene age, which is also a bright radar reflector. Below the Garra is the Kurkur Formation of Paleocene age, which is only locally a bright radar reflector (Fig. 2b); over much of the plateau and on its flanks the Kurkur appears dark, as indicated on the map (c). The ground photo (d) shows a wind-eroded flash flood deposit at locality *A* (b) observed in 1980; the 0.3- to 0.6-m boulders in this deposit are crystalline limestones and other resistant rocks washed down from the scarp and later severely fluted by the wind, to a degree of lacy delicacy suggesting several thousands of years of wind abrasion and deflation in the virtual absence of running water (*17*).

Sahara (*51*). Field observations confirm that the radar-dark areas are dune sand and the radar-bright areas are interdune flats presently deflated to bedrock.

The enhancement of many geologic structures (Fig. 5a) and the delineation of bedrock units partly mantled by sand (Fig. 9a) make the SIR-A radar a valuable adjunct to conventional geologic mapping tools. Because of the radar "look azimuth" problem (*55*), caution must be used in structural mapping, but Fig. 9 shows how the regional distribution of such units as the Dungul, Garra, and Kurkur crystalline limestones of Lower Tertiary age can be better delineated by radar than from Landsat images, on which they appear partly hidden by drift sand. The map of radar units on the Limestone Plateau (Fig. 9c) compares well with the geologic map and descriptions of this region by Issawi (*38*, *56*). Stratigraphic units such as the Dungul and Kurkur Formations have characteristic signatures on the radar images; these signatures are probably due to their different styles of erosion and consequent differences in surface roughness, and thus can be traced across many localities where occurrences are otherwise obscured by the eolian veneer (*11*). In some cases, such as structural depressions and the probable buried intrusives shown on Fig. 5a, infiltration of bedrock crevices by windblown sand and colluvium results in a dark response to SIR-A that enhances the patterns of these structures on radar images. Examples of this phenomenon from other arid regions are given by Elachi *et al.* (*57*).

Those familiar with the Arbain Desert know of tales which date back to ancient Egyptian times and which deal mostly with lost oases such as the legendary "Zerzura" or the great "Bahr-bela-ma" [large river without water (*39*)]. The latter tale prompted Rohlfs (*1*) to undertake the first major European multidisciplinary expedition to the remote western part of Egypt, where he failed to find this legendary (or any other) major river. Before we received the SIR-A data, several of us also passed over many parts of the Arbain Desert with only dim recognition of subtle clues to the existence of major subjacent stream valleys a few meters or less beneath our feet.

Radar backscatter and theoretical considerations. Variations in tone on radar images are caused by changes in radar backscatter that are a function of physical properties of the terrain: slope, roughness, and dielectric constant (Fig. 10). Radar images are related to the average backscattering cross section, σ_0,

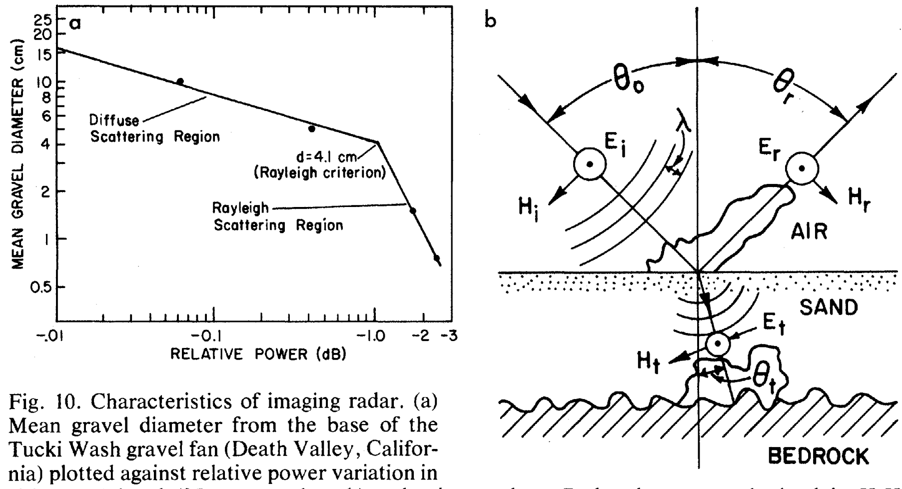

Fig. 10. Characteristics of imaging radar. (a) Mean gravel diameter from the base of the Tucki Wash gravel fan (Death Valley, California) plotted against relative power variation in airborne *L*-band (25-cm wavelength) radar image data. Radar data were obtained in H-H (horizontal transmit–horizontal receive) polarization at an incidence angle of 38° [modified from Schaber *et al.* (*61*)]. (b) Idealized sketch showing reflection (subscripts *r*) and transmission (subscripts *t*) of SIR-A signals incident (subscripts *i*) on radar-smooth sand sheet overlying radar-rough bedrock or buried gravel surface. Horizontal polarization of electric (*E*) and magnetic (*H*) field vectors is shown along with expected scatter patterns (irregular solid lines) from air-sand and sand-bedrock interfaces. Angles are θ_0, incidence; θ_r, reflection; and θ_t, transmission; $\theta_0 = \theta_r$ for a mirror-like surface with scattering facets smaller than $\lambda/10$. Skin depth, δ, is assumed to be in excess of sand thickness [see text and (*60*)].

with lighter tones representing higher σ_0 values and darker tones representing lower ones. For most geologic surfaces, analytic expressions for σ_0 are not available because of simplifying assumptions in the three system and five ground parameters required to calculate σ_0 (*58*):

$$\sigma_0 = f(\lambda, \theta, P, \phi, \epsilon, \tau_1, \tau_2, V) \quad (1)$$

where λ is wavelength; θ, angle of incidence; P, polarization of incident wave; ϕ, aspect angle (terrain slope); ϵ, complex dielectric constant (dominated in most cases by water content and density); τ_1, surface roughness, on microrelief scale greater than $\lambda/10$, of the air-solid interface; τ_2, subsurface roughness of a second layer where the signal can penetrate the first layer to a significant degree; and V, complex volume scattering coefficient in inhomogeneous media.

To properly assess tonal variations on a radar image, one must have at least a qualitative understanding of the effect of each of the parameters listed above for a specific terrain situation. The parameters λ, θ, P, and ϕ are readily available, whereas ϵ and τ_1 can be determined with some certainty within reasonable limits. The values of τ_2 and V are the most difficult to determine even qualitatively, because they involve knowledge of the third dimension of the probed medium. Roth and Elachi (*59*) showed that coherent electromagnetic losses by scattering from volume inhomogeneities (V) can play a more dominant role than conductivity losses. Knowledge of the inferential relations and interactions of all system and ground parameters is extremely difficult to obtain, but some information can be gotten through study of simplified theoretical backscatter models or relevant experimental data.

The Arbain Desert represents a surface where the extremely dry, relatively thin Selima Sand Sheet (Fig. 3b), associated drift sand, and occasional dune fields generally have no microroughness in the form of blocky scatterers over large areas. These deposits are fairly to extremely homogeneous throughout, greatly reducing the contributions of τ_1 and V to σ_0. Thus we have a unique radar-geology situation where the microrelief of the substrate layer, τ_2, may dominate the backscatter return following total penetration of the sand. Where the sand is relatively transparent to the radar signals, σ_0 appears to be dominantly the result of ϵ, τ_2, and electromagnetic losses (because of passage of the waves into and from the medium) that increase with sand thickness. Assuming constant values for ϵ and the loss factors (sand thickness), variations in tone on the radar images will depend primarily on τ_2 (*60*).

A surface (the air-solid interface or a subsurface layer) is "radar-smooth" if it reflects the incident wave specularly in a single direction away from the receiver. A "radar-rough" surface is one that scatters the energy of an incident plane wave in all directions (diffuse scatter). Many natural surfaces exhibit a combination of both types of radar behavior; a surface may be rough for some wave-

Table 2. Characteristics of measured samples from test pits in the Selima Sand Sheet (Fig. 3, b and c).

Sample	Mass (g)	Density (g/cm^3)	Volume (cm^3)	Relative dielectric permittivity, ε	Loss tangent (vacuum-dry), ($\varepsilon_i/\varepsilon_r$)	Attenuation (dB/m)	Skin depth, δ (m)
Granule lag (at surface)	22.75–24.31	1.75–1.87	13	3.34–3.64	0.011–0.029	2.25–6.1	1–6
Eolian sand (1 to 20 cm in depth)	24.05–25.09	1.85–1.93	13	3.20–3.75	0.006–0.043	1.6–9.5	1.5–6
Alluvium (260 to 270 cm in depth)	20.54–21.06	1.58–1.62	13	3.12–3.32	0.011–0.050	2.30–10.0	1–4

lengths and smooth for others, or, for the same wavelength, a surface may be rough or smooth for different antenna depression angles. The transition point between a radar-smooth and radar-rough surface is rather abrupt because it represents a change in scattering processes from Rayleigh scattering to diffuse scattering (Fig. 10a). At the 25-cm wavelength this transition has been shown from empirical measurements of gravel sizes to occur when the mean gravel diameter is about 4 cm for moderate angles of incidence (*61*). The value 4 cm is in excellent agreement with the transition point given by the Rayleigh criterion (*62, 63*):

$$h = \frac{\lambda}{8 \cos \theta} \qquad (2)$$

where h is the height of the irregularities at the transition, λ the radar wavelength, and θ the incidence angle of the radar wave. For a subsurface interface, λ should be replaced by $\lambda/\sqrt{\epsilon}$ and θ by (arc sin $\theta)/\sqrt{\epsilon}$, owing to refraction at the surface (*60*).

The SIR-A system, including the basis for choosing the 24-cm wavelength, 43° depression angle, and 47° incidence angle, is described by Elachi *et al.* (*57*). For the 24-cm wavelength in vacuum (13 cm in sand with $\epsilon = 3.5$) and 47° and 27° incidence angles at the surface and subsurface, respectively, the value of h at the center of the SIR-A image strips is calculated from Eq. 2 to be ~ 4 cm for surface roughness and ~ 2 cm for subsurface roughness. When the scatterers (vertical perturbations or gravels, bedrock, or vegetation) have a mean relief less than about 4 cm on the surface (2 cm in the subsurface) over a planar area that is large with reference to the resolution cell (40 by 40 m), the radar energy is reflected as if the surface were mirror-like (Fig. 2, d, f, g, and h). In such instances the surface or subsurface reflector is not observed on the SIR-A image and the area is dark. When the scatterers are considerably larger, the energy is reflected uniformly in all directions and the area on the SIR-A image is bright (Fig. 2, a to c). In this type of reflection, the radar system receives the noncoherent sum of these reflections, which are scattered back in the direction of the radar antenna. Another type of reflection occurs from a surface that is normally radar-smooth, such as the surface of a sand dune, but has facets (possibly dune slip faces; Fig. 2d) oriented perpendicular to the incident or reflected radar energy; in this case a very bright specular response may be observed (*64*).

Peake and Oliver (*65*) modified the Rayleigh criterion to define surfaces that are clearly radar-smooth and radar-rough [see also (*63*)]. They consider a surface to be radar-smooth (dark on the radar image) if

$$S \leqslant \frac{\lambda}{25 \cos \theta} \qquad (3)$$

where S is the mean height of irregularities of a smooth surface, and radar-rough (bright on the radar image) if

$$R \geqslant \frac{\lambda}{4.4 \cos \theta} \qquad (4)$$

where R is the mean height of irregularities of a rough surface. For the SIR-A images, S and R are 1.4 and 8.0 cm, respectively, at the surface, and 0.7 and 4.0 cm, respectively, at the subsurface interface beneath the loose, dry eolian sand.

The SIR-A image tone resulting from backscatter from the bedrock or gravel surfaces beneath the sand sheets, drift sand, and dunes in Egypt and Sudan may be attenuated more or less directly with the depth of overlying sand if ϵ, and thus the radar penetrability of the sand, remains constant over large areas.

Radar penetration of dry sand and soils. The electrical properties of natural materials and the wavelength of the electromagnetic signals govern the depth of signal penetration into the surface and the ease with which a sympathetic electrical field can be induced in (and hence reradiated from) the surface. Effective penetration depth or "skin depth," δ, of soil or sand varies with the wavelength of the incident signals, incidence angle, and moisture content of the material—the latter determining the electrical properties in most cases.

Electromagnetic energy incident on the surface of a radar-smooth, dry sand sheet would be partly reflected away and partly transmitted (and refracted) through the medium to be diffusely scattered from a rough substrate as shown in Fig. 10b. Moore (*66*) showed that the magnitude of the transmitted electric (or magnetic) field at depth z below the surface, $E_t(z)$, is related to its surface value, $E_t(0)$, by

$$E_t(z) = E_t(0) \exp(-\alpha z \sec \theta_t) \qquad (5)$$

where α is the attenuation coefficient of the sand sheet in nepers per unit length.

For the case of normal incidence ($\theta_t = 0$), δ is defined as the depth at which the total attenuation of the transmitted wave becomes (*66*)

$$\int_0^{\delta} \alpha(z)\, dz = 1 \text{ neper} \qquad (6)$$

It is at this depth δ that the field amplitude of the wave form is reduced to $1/e$ (0.37) of its value at the surface and the power (which is proportional to the square of the field amplitude) reduced to $1/e^2$ (0.135) of the transmitted power at the surface. If the major dielectric discontinuity (such as a bedrock surface beneath the sand) exists at that depth (Fig. 10b), the wave form reflected back to the surface will be further reduced in magnitude by the same amount and will arrive at the surface with a maximum magnitude of only $(0.135)^2 = 0.0183$ of its original value (*67*).

Moore (*66*) pointed out that if $\alpha(z)$ in Eq. 6 is not a function of z, then

$$\delta = 1/\alpha \qquad (7)$$

and if $\theta_t \neq 0$, then z in Eq. 6 must be redefined in terms of the propagation path geometry. The case of $\tau \neq 0$ is shown in Fig. 10b and is representative of the SIR-A image data (center values of $\theta = 47°$) (*60*).

The attenuation coefficient (nepers per meter) can be calculated in terms of the wavelength, real (r) and imaginary (i) components of ϵ, and magnetic permeability μ from

$$\alpha = \frac{2\pi}{\lambda}\left(\frac{\mu\epsilon_r}{2}\left\{\left[1 + \left(\frac{\epsilon_i}{\epsilon_r}\right)^2\right]^{1/2} - 1\right\}\right)^{1/2} \qquad (8)$$

where ϵ_i/ϵ_r is the loss tangent. Ferromagnetics excepted, the magnetic polarization is generally so weak in normal soil and sand that μ may be replaced by the permeability of free space, or unity, for practical purposes (*68*).

The skin depth, δ, in sand, clay, and loam as a function of volumetric moisture content at the 23-cm wavelength was calculated by Myers (*67*) from plots of ϵ_r and ϵ_i against volumetric soil moisture for various soils (*69*) and use of Eqs. 7 and 8 for the expression of α and δ.

Several samples from the Selima Sand Sheet in northern Sudan, collected by C.V.H. and M.J.G. under the SIR-A ground track in February 1982, were available for an initial measurement of dielectric constant and loss tangent. Vacuum-dry measurements of three samples collected from test pits (Fig. 3, b and c) were performed at 1.55 Ghz by Olhoeft (*70*). Results include a typical range for the relative dielectric permittivity (dielectric constant) between 3.1 and 3.7, extremely low loss tangents between 0.006 and 0.05, and attenuation losses between 1.6 and 10.0 dB/m (Table 2). The samples measured were collected from the granule lag at the surface, the underlying eolian sand (sample depth, 1 to 20 cm), and alluvium (sample depth, 260 to 270 cm). The radar skin depth measured for these totally dry samples ranged between 1 and 6 m, with the eolian sand immediately beneath the surface granule lag showing the greatest susceptibility for penetration at the SIR-A wavelength. The samples ranged in density (measured in the laboratory) from 1.6 to 1.9 g/cm^3; 21- to 25-g samples were measured within a volume of 13 cm^3. The measurements were performed in a glove box, using a GR-900 reference coaxial wave guide and a slotted line technique. The thickness, moisture profiles, and electrical properties of the extremely dry Selima Sand Sheet, drift sand, and dunes in Egypt and Sudan will have to be systematically determined over a large area before empirical models of radar backscatter and penetration can be derived or present theoretical models can be tested.

Conclusions. Newly discovered regional, integrated systems of large and small river valleys carved an ancient fluvial landscape that is revealed, by the space shuttle imaging radar, beneath the windblown sand deposits of the Arbain Desert. Such fluvial topography is characteristic of regions with humid climatic conditions and is unrelated to the present hyperaridity in which surface geologic processes are dominated by wind. Fluvial sediments preserved in the buried valleys are marker horizons that record geologic and climatic conditions probably as old as middle Tertiary. Later, during the Quaternary pluvials, parts of these valleys were reutilized by intermittent and finally ephemeral underfit streams. Erosional stripping by rivers during the Tertiary probably accounts for the pediplanation of the Arbain region. This regional denudation was followed by wind beveling of divides and deposition of windblown sand in topographically low valleys and structural depressions. This Quaternary eolian takeover produced an extraordinarily level sand sheet surface that obscures the underlying geologic and topographic features and led to the earlier concept of this surface as an eolian peneplain (*71*). Fluvial activity during the Oligocene and Miocene, interspersed with tectonism and volcanism, thus shaped the erosional evolution of the eastern Sahara. The networks of major river systems that accomplished much of this early denudation are now disrupted and concealed beneath the present eolian surface. These rivers were probably independent of the evolution of the Egyptian Nile. Thus, the old saying that the Nile is Egypt [Herodotus, ~ 450 B.C. (*72*)], while true in a human sense, is not so apt geologically.

Patterns of early human occupation in the Arbain Desert are probably related to the networks of Quaternary wadis that are superimposed on the old Tertiary valleys. As the savanna-like conditions deteriorated with increasing aridity, some of these wadis were gradually reduced to billabong-like, disconnected stretches of standing water that were seasonally replenished. By Holocene time, only scattered playas remained. The search for prehistoric habitation sites has largely centered around these now-abandoned, dry lakes (*43*). Continued mapping of the relict Quaternary drainages as additional radar images are obtained from future shuttle missions should lead to the discovery of numerous additional occupation sites.

Penetration of dry sand and soil to the depths implied by the radar images and supported by calculations based on electrical properties of three samples (Table 2) was considered theoretically possible (*67, 73*) but has been only rarely described (*74*). Few areas on the earth approach the dry barrenness of the hyperarid Arbain Desert. The relict fluvial features in southern Egypt and Sudan resemble features of probable fluvial origin in the northern equatorial region and on the northern plains of Mars (*15*) that also lack running water at present. We can only speculate on the potential of imaging radar to reveal subjacent topography through the dry or frozen eolian veneer that mantles many areas of Mars; electrical properties such as loss tangents appear to be closely similar for parts of the eastern Sahara and the average surface of Mars (*75*). The potential for mapping ancient drainage patterns—and, by inference, potential sources of near-surface ground water—is sufficient to arouse excitement among earth scientists, who now have a new means of exploring the deserts of the earth.

J. F. McCauley
G. G. Schaber
C. S. Breed
M. J. Grolier

U.S. Geological Survey, Flagstaff, Arizona 86001

C. V. Haynes

Department of Anthropology and Geosciences, University of Arizona, Tucson 85721

B. Issawi

Egyptian Geological Survey and Mining Authority, Cairo

C. Elachi
R. Blom

Jet Propulsion Laboratory, California Institute of Technology, Pasadena 91103

References and Notes

1. G. Rohlfs, *Drei Monate in der Libyschen Wüste* (Theodor Fischer, Kassel, 1875).
2. C. V. Haynes, *NASA Contract. Rep. CR3611*, in press.
3. M. A. J. Williams and H. Faure, Eds., *The Sahara and the Nile: Quaternary Environments and Prehistoric Occupation in Northern Africa* (Balkema, Rotterdam, 1980).
4. E. M. V. Bakker, Sr., and J. A. Coetzee, Eds., *Paleoecology of Africa:* vol. 12, *Sahara and Surrounding Seas: Proceedings of International Symposium* (Balkema, Rotterdam, 1980).
5. Geologic Map of Egypt (Egyptian Geological Survey and Mining Authority, Cairo, 1981).
6. B. Issawi and U. Jux, *Egypt. Geol. Surv. Pap. 64* (1982).
7. J. F. McCauley, C. S. Breed, F. El-Baz, M. I. Whitney, M. J. Grolier, A. W. Ward, *J. Geophys. Res.* **84**, 8222 (1979).
8. J. F. McCauley, C. S. Breed, M. J. Grolier, F. El-Baz, *Geogr. J.* **146** (part 1), 84 (1980).
9. F. Wendorf and R. Schild, *Prehistory of the Eastern Sahara* (Academic Press, New York 1980).
10. F. El-Baz, C. S. Breed, M. J. Grolier, J. F. McCauley, *J. Geophys. Res.* **84**, 8205 (1979); F. El-Baz *et al.*, *Geogr. J.* **146**, 51 (1980).
11. In late September 1982 we had the opportunity, in cooperation with the Egyptian Geological Survey and Mining Authority, to conduct a field reconnaissance of parts of the SIR-A swath in Egypt. Numerous test pits were dug in the eolian veneer and in some of these alluvium was found. At one locality along a "radar river" artifacts from all three of the known occupation episodes were discovered, along with middle Paleolithic implements in a gravel lens about 0.5 m below the sand surface. On the Limestone Plateau (locality *X*, Fig. 9), SIR-A backscatter was verified from a rough bedrock substrate below 1.1 m of drift sand and fine colluvium. In general, the observations and interpretations contained in this report were confirmed, particularly the ability of SIR-A to delineate subsurface features below the eolian sand mantle.
12. C. V. Haynes, Jr., *Science* **217**, 629 (1982).
13. C. S. Breed, J. F. McCauley, M. J. Grolier, *NASA Tech. Memo. 82385* (1980), pp. 307–311.

14. C. S. Breed, J. F. McCauley, M. J. Grolier, *Geophys. Res.*, in press.
15. J. F. McCauley, C. S. Breed, M. J. Grolier, *NASA Tech. Memo. 82385* (1980), pp. 312–313.
16. P. S. Chavez, Jr., G. L. Berlin, W. B. Mitchell, in *Proceedings, Sixth Symposium on Remote Sensing of Earth Resources* (Tullahoma, Tennessee, March 1977), pp. 259–275.
17. J. F. McCauley, C. S. Breed, M. J. Grolier, *NASA Contract. Rep. CR3611*, in press.
18. B. Issawi, abstract of papers presented at the Geological Society of America Annual Meeting, New Orleans, 19 October 1982.
19. H.-J. Pachur, in *The Geology of Libya, Second Symposium on the Geology of Libya, Tripoli, 16 to 21 September 1978*, M. J. Salem and M. T. Busrewil, Eds. (Academic Press, New York, 1980), vol. 3, pp. 781–788.
20. R. Said, *The Geological Evolution of the River Nile* (Springer-Verlag, New York, 1981).
21. K. W. Butzer and C. L. Hansen, *Desert and River in Nubia: Geomorphology and Prehistoric Environments at the Aswan Reservoir* (Univ. of Wisconsin Press, Madison, 1968).
22. L. Berry and A. J. Whiteman, *Geogr. J.* **134**, (part 1), 1 (1968).
23. F. W. Van Eysinga, *Geological Timetable* (Elsevier, New York, 1975).
24. R. F. Giegengack, thesis, Yale University (1968).
25. F. Hassan, *Quat. Res. (N.Y.)* **6**, 425 (1976).
26. A. T. Grove and A. Warren, *Geogr. J.* **134** (part 2), 194 (1968).
27. M. Servant and S. Servant-Vildary, in (*3*), pp. 133–162.
28. D. Adamson and F. Williams, in (*3*), pp. 225–252.
29. W. B. K. Shaw, *Geogr. J.* **87**, 193 (1936).
30. M. A. J. Williams, D. A. Adamson, F. M. Williams, W. H. Morton, D. E. Parry, in (*3*), pp. 305–337.
31. G. A. Boulenger, *Nature (London)* **72**, 413 (1905).
32. O. H. Stigand, *Geogr. J.* **48**, 145 (1916).
33. A. Holmes, *ibid.*, p. 149.
34. J. Maley, *C. R. Acad. Sci. Ser. D* **276**, 1673 (1973).
35. E. Raisz, Land Form Map of North Africa, 48 by 22 inches (Boston, Mass., 1952).
36. J. F. McCauley, in *Mantles of the Earth and Terrestrial Planets*, S. K. Runcorn, Ed. (Interscience, New York, 1967), pp. 431–460.
37. D. E. Wilhelms and J. F. McCauley, Geological Map of the Near Side of the Moon: U.S. Geological Survey, Geologic Atlas of the Moon, Near Side of the Moon, Map I-703 (scale 1:5,000,000).
38. B. Issawi, *Gen. Egypt. Org. Geol. Res. Min. Geol. Surv. Pap.* **46** (1969).
39. J. Ball, *Geogr. J.* **70**, 105 (1927).
40. W. J. E. van de Graaff, R. W. A. Crowe, J. A. Bunting, M. J. Jackson, *Z. Geomorphol.* **21** (No. 4), 379 (1977).
41. F. Wendorf, R. Schild, R. Said, C. V. Haynes, A. Gautier, M. Kobusiewicz, *Science* **193**, 103 (1976).
42. F. Wendorf and Members of the Combined Prehistoric Expedition, *Geogr. J.* **143** (part 2), 211 (1977).
43. C. V. Haynes, P. J. Mehringer, Jr., S. A. Zaghloul, *Geogr. J.* **145**, 437 (1979).
44. W. P. McHugh, "Late Prehistoric cultural adaptation in Southwest Egypt and the problem of the Nilotic origins of Saharan cattle pastoralism," *J. Am. Res. Ctr. Egypt* **11**, 9 (1974).
45. W. P. McHugh, *Geogr. J.* **146**, 64 (1980).
46. ———, *NASA Contract. Rep. CR 3611*, in press.
47. G. Caton-Thompson and E. W. Gardner, *Geogr. J.* **80**, 369 (1932).
48. J. D. Clark in (*3*), pp. 527–582.
49. A. B. Smith, in (*3*), pp. 489–501.
50. E. M. Eliason, P. S. Chavez, Jr., L. A. Soderblom, *Geology* **5** (No. 2), 231 (1974).
51. C. S. Breed, N. S. Embabi, H. A. El-Etr, M. J. Grolier, *Geogr. J.* **146**, 88 (1980); C. S. Breed and T. Grow, *U.S. Geol. Surv. Prof. Pap. 1052* (1979), pp. 253–302.
52. A. Warren, *Z. Geomorphol. Suppl.* **10**, 154 (1970).
53. J. R. Parsons, *Am. Antiq.* **33**, 80 (1968); ——— and N. P. Psuty, *ibid.* **40**, 259 (1975).
54. D. Henning and H. Flohn, *Climate Aridity Index Map: United Nations Conference on Desertification* (U.N. Environment Programme, Nairobi, Kenya, 1977).
55. C. Elachi, *Science* **209**, 1073 (1980).
56. B. Issawi, *Ann. Geol. Surv. Egypt* **1**, 53 (1971); ———, *ibid.* **3**, 25 (1973).
57. C. Elachi *et al.*, *Science*, **218**, 996 (1982).
58. J. E. Estes and D. S. Simonett, in *Manual of Remote Sensing*, R. C. Reeves, Ed. (American Society of Photogrammetry, Falls Church, Va. 1975), vol. 2, pp. 869–1076.
59. L. E. Roth and C. Elachi, *IEEE Trans. Antennas Propag.* **23**, 674 (1975).
60. C. Elachi, L. E. Roth, G. G. Schaber, *ibid.*, in press.
61. G. G. Schaber, G. L. Berlin, W. E. Brown, Jr., *Geol. Soc. Am. Bull.* **87**, 29 (1976).
62. P. Beckmann and A. Spizzichino, *The Scattering of Electromagnetic Waves from Rough Surfaces* (Macmillan, New York, 1963).
63. F. F. Sabins, *Remote Sensing, Principles and Interpretation* (Freeman, San Francisco, 1978).
64. R. Blom and C. Elachi, *J. Geophys. Res.* **86**, 3061 (1981).
65. W. H. Peake and T. L. Oliver, "The response of terrestrial surfaces at microwave frequencies:" *U.S. Air Force Avionics Lab. Rep. AFAL-TR-70-301* (1971).
66. R. K. Moore, in *Manual of Remote Sensing*, R. G. Reeves, Ed. (American Society of Photogrammetry, Falls Church, Va., 1975), vol. 1, pp. 399–538.
67. V. I. Myers, in *Manual of Remote Sensing*, R. G. Reeves, Ed. (American Society of Photogrammetry, Falls Church, Va., 1975), vol. 2, pp. 1715–1813.
68. A. R. Von Hippel, *Dielectrics and Waves* (Wiley, New York, 1954).
69. J. Chilar and F. T. Ulaby, *CRES Tech. Rep. 177-47 Univ. Kans. Cent. Res. (Lawrence, Kans.)* (1974).
70. G. Olhoeft, personal communication.
71. K. S. Sandford, *Geogr. J.* **82**, 210 (1933).
72. H. Cary, Transl., *The Histories of Herodotus*, book 2, *Euterpe* (Appleton, New York, 1899), pp. 86–87.
73. J. R. Lundien, *U.S. Army Eng. Waterways Exp. Stn. (Vicksburg, Miss.) Tech. Rep. 3-693* (1971).
74. L. F. Dellwig, *Mod. Geol.* **1** (No. 1), 65 (1969).
75. D. W. Strangway and G. R. Olhoeft, *Philos. Trans. R. Soc. London* **285**, 441 (1977).
76. J. Dubief, in *Die Sahara und ihre Randgebiete*, vol. 1, *Physiogeographie*, H. Schiffers, Ed. (Weltforom, Munich, 1971), pp. 227–348.
77. E. W. Gardner, *Q. J. Geol. Soc. London* **91**, (part 4), 479 (1935).
78. G. W. Murray, *Geogr. J.* **117**, 422 (1951).
79. Work described in this report was carried out under the auspices of the National Aeronautics and Space Administration Office of Non-Renewable Resources and the Planetary Program. Field support was provided by the Smithsonian Institution Foreign Currency Program in cooperation with the Egyptian Geological Survey and Mining Authority and Ain Shams University, Cairo. Support was also provided by the U.S. Geological Survey Office of International Geology and by the Geologic Framework Program. G. Olhoeft measured the electrical properties of our field samples. We thank F. Wendorf and members of the Combined Prehistoric Expedition for their hospitality in the field and W. P. McHugh, E. M. Shoemaker, B. Lucchitta, and D. Scott for their review of the manuscript and their helpful suggestions. W. P. McHugh accompanied us into the Arbain Desert in September 1982 to document relations of the radar subsurface topography to archeological remains.

20 August 1982; 10 October 1982

Mineral Identification from Orbit: Initial Results from the Shuttle Multispectral Infrared Radiometer

Abstract. *A shuttle-borne radiometer containing ten channels in the reflective infrared has demonstrated that direct identification of carbonates and hydroxyl-bearing minerals is possible by remote measurement from Earth orbit.*

The shuttle multispectral infrared radiometer (SMIRR) (*1*) (Fig. 1) was designed to obtain surface reflectance data in ten spectral bands (Fig. 2) in order to evaluate the usefulness of a future imaging system for remote mineral identification. In particular, the region 2.0 to 2.4 μm, which has a wealth of spectral absorption features, appeared to have potential for the identification of CO_3- and OH-bearing minerals such as clays (*2*).

SMIRR was carried aboard the second flight of the shuttle, on 12 to 14 November 1981. Of 186 minutes of data acquired, approximately 70 minutes, equivalent to 400,000 ten-channel spectra, were obtained under totally cloud-free conditions. Another 50 minutes of data were acquired in apparently cloud-free conditions, but the presence of high thin clouds cannot be ruled out (Fig. 3).

Two types of calibration procedures were applied to SMIRR. Absolute calibration of the instrument was carried out in the laboratory by use of a calibrated light source referenced to a National Bureau of Standards standard. Calibration during flight was performed by use of internal lamps. Before SMIRR was installed on the payload pallet, aircraft (*3*) and ground tests were conducted to determine its response to known targets. Figure 4 shows the results of laboratory tests with two clay minerals known to absorb between 2 and 2.5 μm. Continuous laboratory spectra were obtained with a Beckman 5240 spectrophotometer (*4*) modified for digital recording. In order to obtain spectral reflectance within the SMIRR filter bandpasses, the continuous spectra were weighted with filter transmission spectra produced on the same instrument according to

$$\frac{\sum_{n=1}^{k} F(\lambda_n)\, C(\lambda_n)}{\sum_{n=1}^{k} F(\lambda_n)}$$

where $F(\lambda_n)$ is the filter transmission, $C(\lambda_n)$ is the continuous spectrum of the sample measured in n intervals, and k is the number of intervals needed to cover the complete filter bandpass. Calibration tests were performed outdoors with pure mineral samples to determine the correspondence between SMIRR and laboratory measurements. Figure 5 shows the ten-channel spectra developed from continuous laboratory data and measurements made with the sun as a source. The difference in absolute reflectance between the laboratory and SMIRR mea-